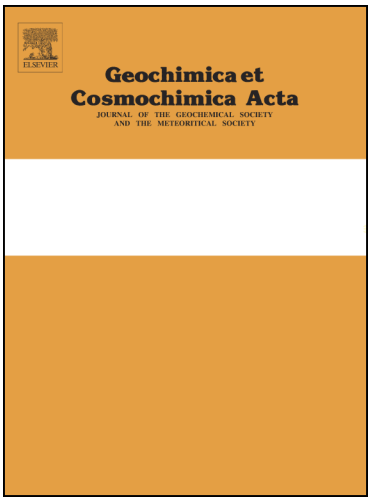

Carbonic anhydrase, coral calcification and a new model of stable isotope vital effects

Sang Chen, Alexander C. Gagnon, Jess F. Adkins

PII: S0016-7037(18)30114-5
DOI: https://doi.org/10.1016/j.gca.2018.02.032
Reference: GCA 10675

To appear in: *Geochimica et Cosmochimica Acta*

Received Date: 13 June 2017
Accepted Date: 16 February 2018

Please cite this article as: Chen, S., Gagnon, A.C., Adkins, J.F., Carbonic anhydrase, coral calcification and a new model of stable isotope vital effects, *Geochimica et Cosmochimica Acta* (2018), doi: https://doi.org/10.1016/j.gca.2018.02.032

Carbonic anhydrase, coral calcification and a new model of stable isotope vital effects

Sang Chen (corresponding author: scchen@caltech.edu)

Division of Geological and Planetary Sciences, California Institute of Technology, Pasadena, CA 91125

Alexander C. Gagnon

The School of Oceanography, University of Washington, Seattle, WA 98195-7940

Jess F. Adkins

Division of Geological and Planetary Sciences, California Institute of Technology, Pasadena, CA 91125

Abstract

The stable isotope compositions of biogenic carbonates have been used for paleoceanographic and paleoclimatic reconstructions for decades, and produced some of the most iconic records in the field. However, we still lack a fully mechanistic understanding of the stable isotope proxies, especially the biological overprint on the environmental signals termed "vital effects". A ubiquitous feature of stable isotope vital effects in marine calcifying organisms is a strong correlation between $\delta^{18}O$ and $\delta^{13}C$ in a range of values that are depleted from inorganic calcite/aragonite. Two mechanisms have been proposed to explain this correlation, one based on kinetic isotope effects during $CO_2(aq)$-HCO_3^- inter-conversion, the other based on equilibrium isotope exchange during pH dependent speciation of the dissolved inorganic carbon (DIC) pool. Neither mechanism explains all the stable isotope features observed in biogenic carbonates. Here we present a fully kinetic model of biomineralization and its isotope effects using deep-sea corals as a test organism. A key component of our model is the consideration of the enzyme carbonic anhydrase in catalyzing the $CO_2(aq)$-HCO_3^- inter-conversion reactions in

the extracellular calcifying fluid (ECF). We find that the amount of carbonic anhydrase not only modulates the carbonate chemistry of the calcifying fluid, but also helps explain the slope of the $\delta^{18}O$-$\delta^{13}C$ correlation. Differences in CA activity in the biomineralization process can possibly explain the observed range of $\delta^{18}O$-$\delta^{13}C$ slopes in different calcifying organisms. A mechanistic understanding of stable isotope vital effects with numerical models can help us develop better paleoceanographic tracers.

Key Words: stable isotope vital effects; $\delta^{18}O$-$\delta^{13}C$ slope; kinetic isotope effects; carbonic anhydrase; deep-sea corals

1. Introduction

The oxygen isotope composition of biogenic carbonates has been established as a proxy for past climate change for decades, since Urey (1947) first worked out the theoretical bases of the ^{18}O thermometer. The proxy is based on the temperature-dependent equilibrium isotope fractionation between carbonates and the fluid from which they precipitated. The successful application of the ^{18}O thermometer in biogenic carbonates relies on the assumption of equilibrium isotope fractionation, or at least a constant offset from equilibrium for the same category of organisms. However, disequilibrium isotope effects between carbonate and water have been widely observed in both laboratory experiments and natural samples. In the first experimental demonstration of the applicability of the ^{18}O thermometer in carbonates, McCrea (1950) noticed the dependence of the isotopic composition of the precipitated calcite on the percentage of carbonate ion in the solution at a constant temperature and $\delta^{18}O$ of water. This carbonate ion effect on the oxygen isotope composition of carbonates was later explained by oxygen isotope partitioning between the dissolved inorganic carbon (DIC) species (Usdowski &

Hoefs, 1993; Beck et al., 2005), and was suggested by Zeebe (1999a) to cause the non-equilibrium oxygen isotope fractionation observed in inorganic experiments (Kim & O'Neil, 1997) as well as cultured foraminifera (Spero et al., 1997). An insight from the interpretation of Zeebe (1999a) is the necessity to incorporate all the DIC species into the solid phase to explain its isotopic composition, making the carbonate-water fractionation ($\alpha_{c\text{-}w}$) a function of pH of the solution in addition to temperature. Follow-up work on this subject also observed a decrease of $\alpha_{c\text{-}w}$ with increasing growth rate of calcite (Gabitov et al., 2012; Watkins et al., 2013) and aragonite (Gabitov, 2013), suggesting kinetic isotope effects (KIE) from ion adsorption and desorption at the solution-solid interface during carbonate precipitation. This growth rate effect can cause an offset of the isotopic composition of the solid from the DIC pool (Watkins et al., 2014).

In addition to the temperature and pH dependent thermodynamic fractionation and growth rate dependent kinetic fractionation, the isotope exchange between the DIC species and water brings another source of disequilibrium, due to the relatively slow rate of CO_2(aq)-HCO_3^- inter-conversion. Although the timescale for one CO_2(aq)-HCO_3^- inter-conversion cycle is on the order of a minute at seawater pH, many cycles are required to achieve a complete exchange of oxygen atoms between the DIC species and water to reach isotope equilibrium (McConnaughey, 1989b). As a result, the equilibration timescale for oxygen isotopes in the DIC pool (hours to days) is significantly longer than for carbon isotopes (seconds to minutes), especially at high pH when the CO_2(aq)-HCO_3^- inter-conversion approaches an irreversible reaction (McConnaughey, 1989b; Zeebe & Wolf-Gladrow, 2001). The oxygen isotope equilibration timescale is longer than most natural calcification processes, as well as many laboratory experiments, which could lead to a significant expression of KIEs during hydration and hydroxylation of CO_2 and subsequently in

the resulting carbonates. Carbon isotopes also experience KIEs during DIC speciation, but to a smaller extent than oxygen. The KIEs of hydration/hydroxylation were proposed by McConnaughey (1989a,b) to explain the strong correlation between $\delta^{18}O$ and $\delta^{13}C$ observed in a variety of marine calcifying organisms growing under the same environmental conditions (Figure 1). McConnaughey (1989a) also pointed out the role of photosymbionts on the carbon isotope composition of coral skeletons, making the $\delta^{13}C$ more enriched compared to non-symbiotic corals.

The KIE mechanism by McConnaughey (1989a,b) predicts a simple linear relation between $\delta^{18}O$ and $\delta^{13}C$ in biogenic carbonates with a particular slope. A challenge to this mechanism was raised from a study of deep-sea corals (*Desmophyllum dianthus*), which observed a break in the $\delta^{18}O$- $\delta^{13}C$ linear relation at the most isotopically depleted end (Adkins et al., 2003). The optically dense central bands in these deep-sea corals, called centers of calcification (COCs), have similar $\delta^{13}C$ to the most depleted values in the surrounding aragonite fibers, but are more depleted in $\delta^{18}O$ than the secondary aragonite. The unique composition of the COCs causes a kink in the $\delta^{18}O$-$\delta^{13}C$ relation (Figure 1a), which led Adkins et al. (2003) to propose a different mechanism for the stable isotope vital effects (Figure 2). This mechanism was based on the observed pH up-regulation in corals within their ECF by the enzyme Ca-ATPase (Al-Horani et al., 2003; Venn et al., 2011). As Ca-ATPase pumps Ca^{2+} into the ECF in exchange for two protons, the pH of the ECF is raised, which shifts the DIC speciation towards the ^{18}O-depleted carbonate ion. Simultaneously, decreasing $CO_2(aq)$ concentration in the ECF causes a larger ^{13}C-depleted CO_2 flux from the calicoblastic cells into the ECF, as opposed to ^{13}C-enriched DIC from the seawater leak. The simultaneous depletion of $\delta^{18}O$ and $\delta^{13}C$ during pH up-regulation stops when the pH of ECF reaches a threshold (pK_{a2}). After pK_{a2}, $CO_2(aq)$ in

the ECF is so low that the cell CO_2 flux is maximized, while the DIC speciation keeps moving from bicarbonate to carbonate ion, promoting further depletion of $\delta^{18}O$ in the $CaCO_3$. This is hypothesized to explain the $\delta^{18}O$-$\delta^{13}C$ kink produced by the COCs. In this model, however, Adkins et al. (2003) assumed equilibrium isotope fractionation between the DIC species. The neglect of KIEs during oxygen isotope exchange caused their numerical model to have a steeper $\delta^{18}O$-$\delta^{13}C$ slope than the observed range in deep-sea corals (1.9-2.6). In addition, the isotopic composition of the skeleton predicted by the composition of the DIC pool is offset from the expected inorganic aragonite values. This begs a new model of biomineralization to explain the observed $\delta^{18}O$-$\delta^{13}C$ data that takes into account the KIEs during DIC speciation, and applies the correct fractionation between the carbonate, DIC species and water.

Here we present a numerical model of coral calcification modified from Adkins et al. (2003). The fundamental components of the model are based on biological and geochemical observations of the coral calcification process, most of which were also considered in McConnaughey's seminal work (McConnaughey, 1989a, b). As observed in calcein and trace metal labeling experiments, seawater is directly involved in the coral calcification process (Tambutte et al., 2012; Gagnon et al., 2012). In our model, we treat ambient seawater as the starting material of the ECF, the composition of which the corals constantly modify. Corals actively up-regulate the pH of their ECF relative to ambient seawater, to locally increase saturation state and calcification rate, as suggested by direct pH measurements (e.g. Al Horani et al., 2003; Venn et a., 2011) and boron isotopes (e.g. McCulloch et al., 2012; Wall et al., 2015). Ca-ATPase, an enzyme that exchanges protons for calcium ions, plays an important role in the pH up-regulation, and has been localized in the calicoblastic cells (Zoccola et al., 2004). In addition, our model considers the role of the enzyme carbonic anhydrase (CA) in the coral

calcification process. CA is a ubiquitous enzyme found in almost all living organisms that catalyze the CO_2-HCO_3^- inter-conversion (Bertucci et al., 2013). The role of CA in the calcification process of corals has been suggested from CA-inhibition experiments for decades (Goreau, 1959), but it was only in the last decade that CA has been immunolocalized in the coral ECF and skeleton (Tambutte et al., 2007; Moya et al., 2008; Mass et al., 2014). Although these studies have only been performed on a few coral species, the presence of CA in the calcifying space of both symbiotic (*Stylophora pistillata*) and azooxanthellate (*Tubastrea aurea*) corals, as well as evidence for its influence on the calcification of other species, suggest that it is directly involved in the biomineralization of many scleractinian corals (Tambutte et al., 2007; Moya et al., 2008; Bertucci et al., 2013; Mass et al., 2014). Consideration of carbonic anhydrase in the model represents an important difference from both the McConnaughey (1989a,b) model and the Adkins et al. (2003) model. The two previous models can be regarded as two limits of CA activity in the ECF, with the McConnaughey model corresponding to zero CA activity, and the Adkins model corresponding to infinite CA activity. The effect of CA activity on the carbonate chemistry of the ECF is detailed in the model results section. Finally, debates remain about the relative importance of paracellular seawater transport versus transcellular ion pumping during coral biomineralization (Tambutte et al., 2011; Tambutte et al., 2012; Gagnon et al., 2012), and the degree to which the calcification process is physicochemically or biologically controlled (Cuif & Dauphin, 2005; Venn et al., 2011; Allison et al., 2014; Mass et al., 2014; Von Euw et al., 2017). Instead of considering the complicated biological processes at a molecular level, our quantitative model treats the major biological processes as fluxes associated with carbonate chemistry, to test the applicability of simple physicochemical rules to tracers in biogenic carbonates.

Deep-sea corals are good test organisms of a stable isotope model given their relative lack of environmental variability and the full range of $\delta^{18}O$ and $\delta^{13}C$ disequilibria observed in their skeletons. Our biomineralization model takes into account different processes during coral calcification that fractionate carbon and oxygen isotopes. In particular, the model tracks the kinetics of CO_2 hydration and hydroxylation in the ECF and its isotope effects under different alkalinity pump rates and ECF pH values. By comparing model results to stable isotope data, the model provides a test of the McConnaughey and Adkins ideas. In addition, the presence of CA in the ECF can facilitate oxygen isotope equilibrium among the DIC species, as has been demonstrated in inorganic precipitation experiments (Uchikawa & Zeebe, 2012; Watkins et al., 2014). As discussed in the model results, accounting for CA activity in the ECF is important in explaining the stable isotope vital effects in deep-sea corals and potentially other calcifying organisms. Finally, the model also applies an offset in the isotopic composition of the carbonate skeleton from the DIC pool for both carbon and oxygen isotopes based on inorganic precipitation experiments and the ion-by-ion growth model (Romanek et al., 1992; Watkins et al., 2014; Watkins & Hunt, 2015). By applying the isotope fractionation factors determined in inorganic experiments to biogenic carbonates, we intend to explore the extent to which vital effects can be explained with fundamental physical chemistry rules. With the major fractionation processes considered above, the model is not only expected to better simulate the deep-sea coral data, but also to explain the range of $\delta^{18}O$-$\delta^{13}C$ slopes observed in different marine calcifying organisms (Figure 1).

2. Method

A schematic diagram of the deep-sea coral based ECF model is shown in Figure 2. The model is modified from the McConnaughey and Adkins models, based on the ubiquitous observation that corals up-regulate their ECF pH relative to ambient seawater (e.g. Al Horani et al., 2003; Venn et al., 2011; McCulloch et al., 2012; Wall et al., 2015). There are two sources of carbon that end up in the coral skeleton, one from seawater DIC and the other from CO_2(aq) diffusing across the ECF membrane. With an increase the saturation state and calcification rate, corals can be limited by the conversion of CO_2(aq) to bicarbonate and carbonate ions, which is a kinetically slow step due to the reorganization of covalent bonds. There are two ways the rate of this conversion can be biologically enhanced. The first is to increase the pH of the ECF by Ca^{2+}-proton exchange through Ca-ATPase, which lowers CO_2(aq) in the ECF and drives cross-membrane CO_2(aq) fluxes and promotes the faster hydroxylation of CO_2(aq). The second is to synthesize carbonic anhydrase, which directly catalyzes the CO_2(aq) hydration reaction. In our model, we write out the equations of CO_2(aq)-HCO_3^- inter-conversion through both hydration and hydroxylation pathways, and track the time evolution of the chemical species in the ECF as calcification takes place. In particular, we specify an alkalinity pumping rate, and track how alkalinity, different DIC species and [Ca^{2+}] change due to fluxes from hydration/hydroxylation, seawater transport, cell membrane crossing, and calcification. For the DIC species, we assume that the HCO_3^--CO_3^{2-} conversion is instantaneous (10^{-7} s) compared to the slow CO_2(aq)-HCO_3^- conversion (10^2 s) (Zeebe & Wolf-Gladrow, 2001), and combine [HCO_3^-] and [CO_3^{2-}] in the equations as equilibrated inorganic carbon (EIC) pool. In addition, we treat CA activity as a rate enhancement factor (k_{cat}) in the CO_2(aq) hydration reaction. Given the low CO_2(aq) concentration in seawater, the CA-catalyzed hydration can be approximated with first-order kinetics (Uchikawa & Zeebe, 2012). The seawater and cell fluxes are treated as a concentration

gradient driven diffusion process as in Adkins et al. (2003). The calcification rate law is obtained from inorganic aragonite precipitation experiments (Romanek et al., 2011). The differential equations in the model are listed in the appendix. For a given alkalinity pump rate, the forward model is run toward steady state with Matlab's ode15s solver, with seawater composition as the initial condition. The carbonate chemistry of the ECF is updated at each time step with CO2SYS. In our fully kinetic model, the carbonate system of the ECF may not reach equilibrium, due to the kinetic barrier of CO_2(aq)-EIC conversion. However, in the range of pH simulated, CO_2(aq) constitutes less than 1% of DIC at equilibrium, and the maximum CO_2(aq) excess we get from the kinetic barrier is 1.6%. This non-equilibrium effect corresponds to a maximum pH offset of 0.03 units in our CO2SYS calculations, or 7% in H^+ activity, which does not significantly influence our model results.

In order to track the isotope processes with the model, we also write out equations for the ^{13}C and ^{18}O substituted species, with the fractionation factors incorporated in the rate constants. The processes that fractionate isotopes in the model are: CO_2(aq)-HCO_3^- inter-conversion through hydration/dehydration and hydroxylation/dehydroxylation, precipitation of the skeleton from the EIC pool, and CO_2(aq) diffusion across the cell membranes. Both carbon and oxygen isotopes can be fractionated through these processes. There have been relatively reliable constraints on the carbon isotope fractionation factors associated with the related processes (Marlier & O'Leary, 1984; O'Leary et al., 1984; O'Leary et al., 1992; Zeebe & Wolf-Gladrow, 2001), although inconsistencies remain between experimental data and theoretical calculations (Zeebe, 2014). However, the kinetic fractionation factors for oxygen isotopes are not as well constrained, especially for the CO_2(aq) hydration and hydroxylation reactions. As a result, we started with the range of values calculated based on transition state theory (Zeebe, 2014) and

tested the model's sensitivity to the fractionation factors. We find that a range of fractionation factors can fit the data, and the exact values needed to fit the data depend strongly on the CA rate enhancement factor. In addition, we incorporate the pH and growth rate dependence of the carbonate-water oxygen isotope fractionation (Watkins et al., 2014) and carbonate-DIC carbon isotope fractionation (Watkins & Hunt, 2015) to account for the isotope effects of fluid-solid interaction. A fluid-solid ^{13}C and ^{18}O fractionation factor based on pH and $CaCO_3$ precipitation rate is assigned following the ion-by-ion model (Watkins et al., 2014; Watkins & Hunt, 2015) at each time step as the forward model is run toward steady state. In the isotope-enabled fully kinetic model, every given alkalinity pump rate also corresponds to a steady state carbon and oxygen isotope composition of the coral skeleton. A summary of the model parameters and fractionation factors is given in Appendix Table 1.

3. Results

3.1 Carbonate chemistry in the ECF

Figure 3 shows the steady state solutions of the carbonate chemistry species in the ECF at different alkalinity pump rates as a function of Alk-DIC space. The three cases examined are associated with different CA activities in the ECF. The slow kinetics case corresponds to no CA, and the $CO_2(aq)$-HCO_3^- inter-conversion follows inorganic seawater rate constants (Johnson, 1982; Zeebe & Wolf-Gladrow, 2001), as proposed by McConnaughey (1989a,b). In the other extreme, the $CO_2(aq)$-HCO_3^- inter-conversion through hydration/dehydration is instantaneous, as has been examined in the model by Adkins et al. (2003). Between the two extremes, a finite amount of CA activity in the ECF is shown as a 2000 times enhancement of the hydration/dehydration rates. As the alkalinity pump rate is increased, the pH of the ECF is

elevated, and the steady state solutions of DIC and alkalinity in the ECF moves from the lower right to the upper left corner in the Alk-DIC space (Figure 3a). However, the pathways of pH elevation are different in the presence or absence of CA. In the absence of CA, the DIC of ECF first decreases significantly relative to the seawater source while the pH is rapidly elevated, after which there is a small change in DIC as alkalinity is further pumped in. In the presence of CA, however, DIC first starts to increase with a relatively small increase in pH, and then decreases rapidly with rapid pH elevation like the slow kinetics case. In all cases, there is a maximum carbonate ion concentration as the alkalinity pump is turned up (Figure 3b). However, the reasons for the $[CO_3^{2-}]$ increase towards a maximum are different for the different cases. While the CA-absent case gets to a $[CO_3^{2-}]$ maximum solely by increasing pH (and thus the fraction of CO_3^{2-} in DIC), the CA-present cases approaches a $[CO_3^{2-}]$ maximum by the combined effects of DIC and pH increase. The contrast between these cases demonstrates the fundamental role CA plays in the carbon budget and calcification dynamics of the ECF.

3.2 Stable Isotopes

Figure 4 shows the steady state isotope compositions of the skeleton as the alkalinity pump is turned up for the three cases presented in Figure 3. As the pH is elevated with the alkalinity pump, both $\delta^{18}O$ and $\delta^{13}C$ get more depleted. In all cases, there is a kink in the $\delta^{18}O$-$\delta^{13}C$ relation, but the kink shows up more clearly with the presence of CA. In addition, there is a systematic change in slope of the $\delta^{18}O$-$\delta^{13}C$ relationship, with a higher CA activity corresponding to a steeper slope. In the instantaneous kinetics case, the $\delta^{18}O$-$\delta^{13}C$ linear trend is close to being vertical. Data from deep-sea coral 47407 (Adkins et al., 2003) is best fit by a CA rate enhancement of 2000× (Figure 4a). To test the robustness of the model, we also tried to fit

different deep-sea coral datasets by only changing the ambient seawater conditions while holding the other parameters constant (Figure 4b). With the same set of parameters, our model also fits the stable isotope data of two other deep-sea corals. It should be noted that a $\delta^{13}C$ offset of 1‰ was applied to cross-membrane $CO_2(aq)$ for coral 78459 to make the model line go through the data. We suspect this reflects different fractions of ^{13}C-depleted metabolic CO_2 used for calcification. The fraction of metabolic carbon corresponding to a 1‰ $\delta^{13}C$ offset is estimated to be 6-7% of all $CO_2(aq)$, consistent with radiocarbon constraints of a maximum of 6-8% metabolic carbon contribution to the skeleton in *D.dianthus* (Adkins et al., 2002) . The effect of CA on the model fit to the stable isotope data again suggests its important role in the calcification process, and points towards a new mechanism for stable isotope vital effects.

4. Discussion

4.1 CA and ECF carbonate chemistry

As shown above, the steady state DIC and alkalinity responses to increasing alkalinity pump diverge by adding CA to the model. Figure 5 shows the steady state carbonate chemistry variables of the ECF corresponding to different alkalinity pump rates (a different view of Figure 3), and further demonstrates this difference. In the slow kinetics case, the pH of the ECF rises rapidly from the seawater value to a pH of 10 at a very small increase in the pump rate, after which the pH rises more gradually (Figure 5a). These high pH values are dangerous to the corals as they would promote saponification of the lipid membranes. During the rapid pH rise, there is also a sharp decrease in DIC, but the pH effect dominates to drive a $[CO_3^{2-}]$ increase (Figure 5c). When CA is present, however, the pH of the ECF is much more strongly buffered with the alkalinity pump increase. There is a slow pH rise as the pump is turned up from zero until a pH

around 9.3, the value of pK_{a2} at deep-sea coral growth conditions (5°C, 500 m), after which there is a sharp pH rise (Figure 5a). Between seawater pH and pK_{a2}, $[CO_3^{2-}]$ increases until a maximum value at the sharp pH jump (Figure 5c). Corresponding to this maximum $[CO_3^{2-}]$, there is also a dramatic decrease in the slope of the precipitation rate with pump rate (Figure 5f). In the model, $[CO_3^{2-}]$ is the dominant factor controlling the saturation state, and precipitation rate, in the ECF with a factor of 5-6 change, as opposed to $[Ca^{2+}]$ which changes by less than a factor of 2 (Figure 5d). Similar observations have been made in laboratory simulations of the biomineralization process (Zeebe & Sanyal, 2002). It has been previously suggested that pK_{a2} represents an energetic limit of biological pH elevation (Adkins et al., 2003). After pK_{a2}, the additional precipitation rate obtained from the ATP-driven alkalinity pump is minimal, as observed in our model. ECF pH measurements in surface corals have found few cases of pH above pK_{a2} (Al-Horani et al., 2003; Venn et al., 2011; Cai et al., 2016), consistent with this idea. The $[CO_3^{2-}]$ maximum of ~1000 μmol/kg in our model (Figure 5c) also agrees with microelectrode measurements of ECF composition in surface corals (Cai et al., 2016). In addition, there is a range of pump rates in which the DIC of the ECF is elevated relative to seawater (Figure 5e). This biologically controlled DIC elevation in the ECF has been experimentally observed in some surface corals (Allison et al., 2014), but not in others (Cai et al., 2016). The difference in DIC concentrations in the ECF may reflect different alkalinity pump rates or CA activity among the coral species (Figure 5e).

The change in the ECF carbon budget with the presence of CA indicates a larger carbon flux from somewhere. Figure 6 shows the steady state fluxes controlling alkalinity, DIC, and EIC at different pump rates. As expected, the presence of CA drives large hydration and dehydration fluxes (Figure 6f), and an increasing imbalance of the two as the alkalinity pump is turned up.

This imbalance keeps [CO_2(aq)] low in the ECF (Figure 5b), and creates a large [CO_2(aq)] gradient between the cell and ECF. As a result, the CO_2(aq) flux across the cell membrane is higher at low pump rates in the presence of CA (Figure 6e vs. 6b). As CO_2(aq) is rapidly converted to EIC, the cell flux helps concentrate DIC in the ECF, and maintains a relatively high DIC:Alk ratio so that the pH change is much more gradual. This cross-membrane CO_2(aq) flux also explains the DIC elevation in the ECF relative to seawater (Figure 5e), when precipitation is not fast enough to remove all the additional carbon. As the pump rate is further increased, precipitation starts to outcompete the cross-membrane flux to drive DIC down, but [CO_3^{2-}] can keep increasing due to pH elevation (Figure 5c and 5d). In contrast, CO_2(aq) cannot be effectively converted to EIC without CA at low pump rates, causing the ECF to be less buffered and the pH to be very sensitive to small increases in the alkalinity pump. The rapid pH rise in the slow kinetics case then shifts the CO_2(aq)-EIC conversion to the more efficient hydroxylation pathway, causing the cell flux to catch up and the pH to increase more gradually (Figure 6b and 6c). In both the slow kinetics and CA-enhanced cases, there is a maximum cell CO_2(aq) flux, when CO_2(aq) in the ECF cannot be any lower (Figure 5b). After the threshold, the change in the ECF carbon budget can only be modulated by the seawater and precipitation fluxes, which has implications for the stable isotopes in the following discussions. This pH threshold is at pK_{a2} for the CA-enhanced case, as CO_2(aq) can be rapidly converted to EIC. The pH threshold is higher for the slow kinetics case, when there is a kinetic barrier to the CO_2(aq)-EIC conversion.

To summarize, our model has found two important roles CA plays in the biological calcification process as compared to slow kinetics: to concentrate DIC in the ECF for calcification, and to buffer the carbonate system of the ECF against unfavorably high pH as the alkalinity pump increases. CA releases the kinetic barrier to EIC production from CO_2(aq) that

would otherwise pool in the ECF. By synthesizing CA for use in the calcification process, the calcifying organism can get a steady increase in ECF [CO_3^{2-}] and precipitation rate, in a chemical environment that does not saponify membrane lipids.

4.2 Isotope composition of coral skeleton

Figure 4 shows that a finite amount of CA activity generates a stable isotope model line that goes through the deep-sea coral data. A fit to the data requires three features to be correctly simulated: (1) the isotope composition at the $\delta^{18}O$ and $\delta^{13}C$ enriched end (equilibrium limit) of the dataset; (2) the slope of the $\delta^{18}O$-$\delta^{13}C$ linear correlation part; and (3) a kink in the $\delta^{18}O$-$\delta^{13}C$ relation that represents the COCs. The three parts are discussed separately below.

4.2.1 Biogenic vs. inorganic carbonates at the equilibrium limit

While the $\delta^{18}O$ and $\delta^{13}C$ proxies are based on equilibrium isotope effects, several processes can cause disequilibrium isotope effects in both inorganic precipitation experiments and biological calcification. Since the solid carbonate inherits its isotope composition from the DIC pool, the disequilibrium isotope effects can take place either in the DIC speciation process or in the solid formation process. Isotope exchange during DIC speciation is kinetically limited due to the slow CO_2(aq)-HCO_3^- inter-conversion, especially for oxygen isotopes because water is involved in the exchange (McConnaughey, 1989b; Zeebe & Wolf-Gladrow, 2001; Uchikawa & Zeebe, 2012). In the solid formation process, there is additional isotope fractionation due to ions attaching to and detaching from the solid surface, the net effect of which is reflected by the growth rate of the solid (Watkins et al., 2013). As a result, true carbonate-water isotope equilibrium can only be achieved when all the DIC species are in isotope equilibrium, and the

growth of the solid is slow enough to prevent KIEs during precipitation. In a comprehensive survey of this problem, Watkins et al. (2014) used CA to facilitate the DIC species equilibrium, and did inorganic calcite precipitation experiments across a range of temperatures, pH and growth rates, to establish the full dependence of the calcite-water oxygen isotope fractionation on these factors. From the Watkins model, isotope fractionation factors can be obtained between the solid and the two EIC species, bicarbonate and carbonate ions. Similar inorganic precipitation experiments have also been performed for aragonite in seawater, and a new temperature dependent aragonite-water $\delta^{18}O$ fractionation equation was proposed at the equilibrium limit (Wang et al., 2013). Given our assumption that the isotope composition of the coral skeleton is determined by the EIC pool, we applied these fractionation factors to calculate the composition of the skeleton for all pump rates, and their associated $CaCO_3$ precipitation rates. Similar to oxygen isotopes, there is also a carbon isotope fractionation between the EIC species and the resulting solid (Romanek et al., 1992; Watkins & Hunt, 2015). For a pump rate of zero, we expect the model to predict the inorganic $CaCO_3$ isotope composition at the corresponding growth rate, which is within the equilibrium limit in the Watkins model. The solid squares in Figure 4a show the solid-EIC fractionations at the equilibrium limit, with the oxygen isotope fractionation factors from Wang et al. (2013) for aragonite. Applying these offsets between the solid and fluid is necessary to generate a line that goes through the data. Without these fractionation factors, the modeled EIC composition is too depleted in $\delta^{13}C$ and too enriched in $\delta^{18}O$. As a result, the biogenic carbonates provide a confirmation to the fractionation factors derived in inorganic experiments and the ion-by-ion growth model (Wang et al., 2013; Watkins et al., 2014).

4.2.2 CA and the $\delta^{18}O$-$\delta^{13}C$ slope

As observed by McConnaughey (1989a), a wide variety of marine calcifying organisms show a linear correlation between $\delta^{18}O$ and $\delta^{13}C$ with a relatively narrow range of slopes (Figure 1). In our model, we tested a range of CA activities, and observed a systematic change in the $\delta^{18}O$-$\delta^{13}C$ slope, with higher CA activity corresponding to steeper slopes (Figure 4). In our flux balance model, it is possible to disentangle what roles different isotope fractionation processes play in setting the slope. The inset vector plot in Figure 7 shows the five important processes that fractionate carbon and oxygen isotopes from the seawater EIC composition. Two of these processes represent equilibrium isotope effects. The horizontal arrow to the left represents the equilibrium oxygen isotope effect from pH driven DIC speciation. Although the equilibrium carbon isotope compositions of DIC species are different, it is a closed system in terms of isotope exchange, and significant changes in EIC $\delta^{13}C$ can only be caused by a change in total $\delta^{13}C$ of the DIC pool. The $\delta^{13}C$ of the DIC in the ECF is set by the mixing of two carbon pools with distinct $\delta^{13}C$ values: membrane-crossing CO_2(aq) and seawater DIC. With a pH increase in the ECF, a larger contribution from membrane-crossing ^{13}C-depleted CO_2(aq) lowers the $\delta^{13}C$ of DIC, as represented by the vertical downward arrow. The Adkins model for stable isotope vital effects is a coupling of these two equilibrium processes through pH elevation, with a kink in the correlation as the carbon isotope mixing effect is maximized at pK_{a2}.

The other three processes shown in Figure 7 that fractionate isotopes are kinetic processes. Both hydration and hydroxylation of CO_2(aq) create $\delta^{18}O$ and $\delta^{13}C$ depleted EIC, which represent the McConnaughey mechanism of stable isotope vital effects. McConnaughey (1989b) attributed the range of $\delta^{18}O$ and $\delta^{13}C$ observed in biogenic carbonates to different degrees of equilibrium exchange of CO_2(aq) across the ECF membrane. However, since the

timescale for carbon isotope exchange (10-100 s) is much shorter than for oxygen isotopes (10^3-10^4 s) (Zeebe & Wolf-Gladrow, 2001; Uchikawa & Zeebe, 2012), the magnitude of carbon isotope hydration/hydroxylation KIE expressed in the resulting solid is expected to be smaller than the oxygen isotopes, given a DIC residence time of 10^2~10^3 s with respect to precipitation. This changes both the magnitude and angle of the hydration/hydroxylation fractionation vectors. An additional kinetic fractionation process happens during precipitation of the skeleton. According to the ion-by-ion growth model (Watkins et al., 2014; Watkins & Hunt, 2015), the precipitating $CaCO_3$ is enriched in ^{13}C and depleted in ^{18}O relative to the EIC pool in the range of growth rates in our model. This could create a residual EIC that is more depleted in ^{13}C and enriched in ^{18}O through a Rayleigh distillation process by precipitation when carbon supply is limited to seawater at low pump rates and no CA. This process could cause a negative slope in the $\delta^{18}O$-$\delta^{13}C$ correlation, which has not received much consideration in previous models of biomineralization. The Rayleigh process can also give rise to more enriched $\delta^{18}O$ values in biogenic carbonates than inorganic precipitation experiments in the equilibrium limit, although other mechanisms such as rapid incorporation of ^{18}O enriched CO_2(aq) have been suggested to explain observed $\delta^{18}O$ enrichments in organisms like coccolithophore (Hermoso et al., 2014; Hermoso et al., 2016).

The $\delta^{18}O$-$\delta^{13}C$ patterns simulated in our model can be decomposed into the different fractionation processes discussed above (Figure 7). For the slow kinetics case, the coral derives most of its carbon for precipitation from seawater DIC at low pump rates, due to the kinetic barrier of CO_2(aq) hydration and low membrane-crossing CO_2(aq) flux. As a result, the precipitation from seawater DIC causes the Rayleigh effect to be expressed in the $CaCO_3$. The Rayleigh effect dominates the $\delta^{18}O$-$\delta^{13}C$ slope until the pH is high enough for hydroxylation to

efficiently convert CO_2(aq) to HCO_3^-, after which the hydroxylation KIE is expressed. For the instantaneous kinetics case, CA can catalyze rapid CO_2(aq)-HCO_3^- inter-conversion and isotope exchange through hydration/dehydration, so that no hydration KIE is expressed. As a result, what ends up being expressed in the skeleton is the equilibrium isotope effects through pH-driven DIC speciation and carbon source mixing. In the presence of abundant CA, the coral can also take full advantage of the cross-membrane carbon source, so that the Rayleigh effect from precipitation is largely reduced. However, the kink in the $\delta^{18}O$-$\delta^{13}C$ correlation at pK_{a2} makes the slope too steep compared to the deep-sea coral data. The 2000× rate enhancement model case that fits the data in Figure 4 is an intermediate case with a finite amount of CA. In this case, the CO_2(aq) hydration KIE is partly expressed for oxygen isotopes (4‰), and to a lesser extent for carbon isotopes (2‰) due to faster isotope equilibration. The observed 10‰ range in deep-sea coral $\delta^{13}C$ is mostly a result of the mixing of cross-membrane CO_2(aq) and seawater DIC, which accounts for 8‰ of the signal. In our model this data-fitting case suggests that the McConnaughey KIE mechanism dominates the observed $\delta^{18}O$ signal, while the Adkins mechanism explains most of the range in $\delta^{13}C$ and the COC kink in deep-sea corals.

The analysis of the fractionation processes for the data-fitting case also provides clues to the role of CA activity in setting the $\delta^{18}O$-$\delta^{13}C$ slope. CA can enhance the CO_2-EIC inter-conversion and shorten the timescale of DIC oxygen isotope equilibration (Uchikawa & Zeebe, 2012). In laboratory experiments 0.25 μM of CA can shorten the oxygen isotope equilibration timescale by 2-3 orders of magnitude (Uchikawa & Zeebe, 2012; Watkins et al., 2013). As a result, it is expected that the presence of CA in the coral ECF can reduce the magnitude of the oxygen isotope KIE. However, since synthesis of CA costs the coral energy, it is reasonable to assume a finite amount of CA in the ECF, so that the KIE signal of CO_2-EIC conversion is not

totally erased. The forward reactions of hydration/hydroxylation make isotopically depleted EIC, and the backward reactions drive the isotope exchange to equilibrium. A metric for the completeness of oxygen isotope exchange is the ratio of the rate of the reverse reactions to the forward reactions. A ratio of one represents equilibrium exchange, while a small ratio represents significant KIE that makes isotopically depleted EIC. This ratio decreases with pH, because higher pH favors the forward reactions as opposed to the backward reactions. Figure 8b shows how this metric changes with alkalinity pump rate for both the slow kinetics and CA-enhanced cases, and the associated change in oxygen isotopes. We can see that the presence of CA makes the reverse to forward reaction ratio decrease much more gradually with an increasing alkalinity pump, thus reducing the KIEs expressed in the resulting skeleton. In the slow kinetics case, the ratio drops rapidly with increasing pump rate, and the KIEs are much more significant. As a consequence, the magnitude of the KIE driven $\delta^{18}O$ depletion in the slow kinetics case is much larger, and the $\delta^{18}O$-$\delta^{13}C$ slope is shallower for the same range in $\delta^{13}C$. The rate enhancement factor of 2000 that fits the deep-sea coral dataset may represent an optimal amount of CA the organism decided to synthesize for its growth needs and energy budget. At 5°C, the $CO_2(aq)$ hydration rate constant in seawater is 4×10^{-3} s^{-1} (Johnson, 1982), and a 2000 rate enhancement factor would correspond to a rate constant of 8 s^{-1}. Measurements of CA activity in symbiotic corals constrain a Michealis-Menten constant (k_{cat}/K_M) of 4.6-8.3$\times10^7$ $M^{-1}\cdot s^{-1}$, (Moya et al., 2008; Bertucci et al., 2011). The 2000 times rate enhancement requires sub-micromolar CA concentration in the ECF. However, *in vivo* experiments have shown that certain amino acids and amines act as CA activators and increase CA activity (Bertucci et al., 2010). In surface coral tissue homogenate, the measured CA-catalyzed hydration rate constant is ~50 s^{-1}, although it was

unclear how CA activity is distributed between photosynthesis and calcification (Hopkinson et al., 2015). An in-situ measurement of CA activity in deep-sea corals may help test our model.

Given that CA activity changes the slope of the $\delta^{18}O$-$\delta^{13}C$ linear correlation, we can explain the range of $\delta^{18}O$-$\delta^{13}C$ slopes observed in marine calcifying organisms with the natural variability of CA activities. Figure 9 shows a range of CA-induced CO_2 hydration rate enhancements with their associated $\delta^{18}O$-$\delta^{13}C$ slopes in our model. The range of slopes observed in deep-sea corals (1.9-2.6) correspond to a wide range of CA catalyzed rate enhancement (200-2000×). When the environment is changed to surface ocean conditions (T=25°), the CA rate enhancement required for a similar observed $\delta^{18}O$-$\delta^{13}C$ slope range still spans an order of magnitude, between 20 and 200×. With higher temperatures and saturation states in the surface ocean, the precipitation rate is an order of magnitude higher in our model. As a result, it is expected that surface ocean calcifying organisms do not need as much CA, and its associated higher DIC concentration in the ECF. In addition, a temperature rise also facilitates the DIC speciation and oxygen isotope exchange kinetics (Beck et al., 2005; Watkins et al., 2013), which compensates for a lower amount of CA in setting the $\delta^{18}O$-$\delta^{13}C$ slope. Although CA has been shown to influence calcification of many marine calcifying organisms (Hentunen et al., 2000), not every species in Figure 1 has been analyzed for CA in its calcifying region. So caution should be applied in applying our model before the enzyme activity is confirmed or denied. In addition, our model does not account for the effect of photosynthesis on the carbon budget. Photosynthetic organisms, or those with photo-symbionts, can have an additional enrichment in $\delta^{13}C$ due to preferential uptake of ^{12}C in photosynthesis, leading to a shallower $\delta^{18}O$-$\delta^{13}C$ slope (McConnaughey, 1989a), or generally more scattered data.

4.2.3 The $\delta^{18}O$-$\delta^{13}C$ kink

The observation that the isotope compositions of COCs in *D.dianthus* falls off the linear $\delta^{18}O$-$\delta^{13}C$ trend led Adkins et al. (2003) to propose an alternative mechanism for vital effects to McConnaughey's (1989a) KIE interpretation. The distinct isotope compositions of COCs have also been observed in other deep-sea coral species (Rollion-Bard et al., 2003; Blamart et al., 2007; Rollion-Bard et al., 2010), as well as surface corals (Juillet-Leclerc & Reynaud, 2010). Mineralogical analyses of the deep-sea coral skeletons show that both the COCs and the secondary structures are aragonite, but microscopic observations show that the COCs have more random orientation compared to c-axis aligned secondary aragonite (Gladfelter, 1984; Gagnon et al., 2007; Rollion-Bard et al., 2010; Von Euw et al., 2017). In addition to stable isotopes, the COCs also have distinct trace element concentrations compared to the secondary aragonite, including higher Mg/Ca and Li/Ca (Gagnon et al., 2007; Case et al., 2010), and lower B/Ca (Blamart et al., 2007) and U/Ca (Robinson et al., 2006). These observations have led to debate about whether the COCs formed with the same mechanism as the secondary aragonite.

Our stable isotope model can generate a continuous $\delta^{18}O$-$\delta^{13}C$ curve that includes both the linear relation and the kink. As proposed by Adkins et al. (2003), the mechanism of the kink is a maximum in the $\delta^{13}C$ depleted cell CO_2(aq) flux when the pH of the ECF reaches pK_{a2}. After this threshold, the $\delta^{18}O$ can keep getting more depleted due to an increasing imbalance of the forward and reverse CO_2(aq)-EIC inter-conversion reactions, but the $\delta^{13}C$ cannot get more depleted (Figure 8c, d). Instead, the $\delta^{13}C$ in our model gets slightly enriched after pK_{a2} due to an increasing seawater DIC influx.

Although we have a model that explains most of the features in the deep-sea coral stable isotope dataset, some caveats remain that require further investigation. A problem with our

interpretation of COCs as forming from the same calcification mechanism as secondary aragonite is the corresponding pH. In our current model, the depleted $\delta^{18}O$ of the COCs correspond to a pH of 11, which is beyond the $[CO_3^{2-}]_{max}$ in Figure 5, and is also biologically unreasonable in a membrane supported ECF system. There are some other possibilities that could explain the composition of the COC. One is that the COCs formed from calcification rates that are distinctly higher than inorganic experiments during the early life stage of the corals. In order to initiate the calcification process, additional energy may be used by the organisms to synthesize organic templates that facilitate the skeleton growth rate (Cuif & Dauphin, 2005; De Yoreo et al., 2007). If the growth rate of the COCs were an order of magnitude higher than inorganic experiments due to organic templating, we could explain an additional 1‰ depletion in $\delta^{18}O$ in the COC at pK_{a2} (Watkins et al., 2013). An alternative explanation involves the role of amorphous calcium carbonate (ACC) in biomineralization. It has been suggested that calcifying organisms can take advantage of the disordered structure of ACC to increase growth rates at early stages of calcification (Addadi et al., 2003), and later transform ACC into more stable calcite or aragonite. ACC has been observed in a variety of calcifying organisms (Jacob et al., 2008; Gago-Duport et al., 2008; Gong et al., 2012). Although no direct evidence of ACC has been reported for deep-sea corals, the distinct microscopic structure, as well as isotopic and trace element composition of COCs have led some authors to suggest the role of ACC as the precursor phase of the skeleton (Rollion-Bard et al., 2010; Von Euw et al., 2017). The trace element compositions of the coral COCs are in many ways similar to ACC observed in other organisms (Jacob et al., 2008). In addition, a recent study of ACC in speleothems suggests that ACC is depleted in $\delta^{18}O$ relative to companion calcite by 2.4±0.8‰ (Demeny et al., 2016). As a result, the composition of COC aragonite could also be explained as an inherited signal from its ACC

precursor. More detailed studies of the coral skeleton structures and characterization of ACC in biogenic carbonates are required to resolve this problem.

4.3 Parameter sensitivity and other calcifying organisms

We have shown that our model can fit the stable isotope data from several different deep-sea corals with a single set of parameters (Figure 4), and discussed in detail the effect of CA on the $\delta^{18}O$-$\delta^{13}C$ slope. Yet, there are other tunable parameters in our model that may change the results. Two important biological parameters are the diffusivity of CO_2(aq) in the calicoblastic cell membranes, and the rate of seawater DIC turnover in the ECF. These two parameters determine the relative contribution of the two carbon sources for coral calcification, and may have significant impacts on the resulting isotope composition of the skeleton. A seawater DIC turnover timescale that fits the observed range in deep-sea coral $\delta^{13}C$ is 230 seconds for the cell diffusivity we used (Sultemeyer & Rinast, 1996). Figure 10 shows example model outputs corresponding to different cell diffusivities and seawater turnover timescales. Increasing the cell diffusivity or decreasing the seawater turnover timescale can make the pH of the ECF more strongly buffered against the alkalinity pump. Changing the relative rate of these two fluxes also changes the range of $\delta^{13}C$ calculated by the model, due to the distinct isotope composition of the two carbon sources. However, in the parameter range we explored, the difference between the slow kinetics case and the CA-enhanced case always exists (as in Figure 4 and 5). Including CA rate enhancement in our model is necessary to generate reasonable ECF chemistry and stable isotope results that fit the data. In addition, some features in the model are robust with a range of parameter sets, including the maximum in $[CO_3^{2-}]$, the $\delta^{18}O$-$\delta^{13}C$ slope with a particular CA rate enhancement, and a $\delta^{18}O$-$\delta^{13}C$ kink. It should be noted that the kink is a persistent feature in the

model as long as the pH of the ECF reaches pK_{a2} of seawater. The fact that the kink is lacking in other surface calcifying organisms may suggest that they do not raise their pH as much as the deep-sea corals.

Examining the sensitivity of our model to biological parameters may help us understand the isotope composition of other marine calcifiers. Different calcifiers may change their membrane permeability to adjust their carbon budget. The seawater turnover timescales may also be different for different organisms, due to wide variance in the geometry of the calcification space and its access to the surrounding seawater. The seawater turnover timescale has important implications for paleoclimate reconstructions as it determines how much of the ambient environmental signal can be recorded in the biogenic carbonates. For example, in a culture experiment by Spero et al. (1997), it was observed that both $\delta^{18}O$ and $\delta^{13}C$ in foraminifera shells decreased with increasing carbonate ion concentration in the ambient seawater. The slope of $\delta^{18}O$ vs. $[CO_3^{2-}]$ was explained by Zeebe (1999a) as the equilibrium isotope effect of pH-driven DIC speciation, and modified by Watkins et al. (2014) as a combined effect of pH and carbonate growth rate. The slope of $\delta^{13}C$ vs. $[CO_3^{2-}]$ in the culture experiment, however, varies from -0.006‰ to -0.014‰ per μmol/kg $[CO_3^{2-}]$ between different species, and is steeper than the $\delta^{18}O$-$[CO_3^{2-}]$ slope of -0.002‰ per μmol/kg $[CO_3^{2-}]$. In our model, the $\delta^{13}C$-$[CO_3^{2-}]$ slope can be simulated at a constant alkalinity pump rate, when the seawater turnover timescale is shortened to <100 s, the CA rate enhancement factor is <100, and with a significant amount (>50%) of $\delta^{13}C$-depleted metabolic CO_2 involved in the calcification process. In this case, the cell CO_2(aq) flux can respond readily to changes in seawater CO_2(aq) in the culture conditions. The necessity to include metabolic CO_2 to produce the $\delta^{13}C$ vs. $[CO_3^{2-}]$ slope is consistent with a diffusion-reaction model proposed by Zeebe et al. (1999b), although their model requires a response of

respiration to changes in ambient Alk:DIC ratio. The more rapid seawater turnover in foraminifera suggested by our model may also explain why their shells are good paleoceanographic archives. Details of a foraminifera based calcification model will be presented in a separate paper.

Conclusions

We have developed a fully kinetic model of biomineralization based on deep-sea corals that can explain the trends in skeletal $\delta^{18}O$ and $\delta^{13}C$. We found that carbonic anhydrase plays an important role in the calcification process, because it buffers the pH and concentrates carbon in the ECF. The existence of carbonic anhydrase also influences the oxygen isotope exchange kinetics, and changes the $\delta^{18}O$-$\delta^{13}C$ slope in the skeleton. A particular $CO_2(aq)$ hydration rate enhancement by CA in the model produces a tight fit to the deep-sea coral stable isotope data, when the correct fractionation factors between the solid carbonate and DIC species are applied. This fit works across multiple different deep-sea corals with minimal changes in the model parameters. Variability in natural CA activity may explain the range of $\delta^{18}O$-$\delta^{13}C$ slopes observed in different marine calcifying organisms. In addition, the kink in $\delta^{18}O$-$\delta^{13}C$ found in COCs of deep-sea corals is a robust feature of pH up-regulation beyond pK_{a2} in our model, the mechanism of which requires further investigation. The extension of our model to organisms other than deep-sea corals shows some prospects for a ubiquitous mechanism for stable isotope vital effects. Better biomineralization models with carbonate chemistry dynamics can not only help us develop better paleoceanographic tracers, but also advance our understanding of biological calcification response to future climate change.

Acknowledgments

This work received support from NSF grant P2C2-1503129. S.C. would like to acknowledge financial support from the China Scholarship Council for Ph.D. study at Caltech. We would also like to thank James Watkins for sharing his Matlab code for the oxygen isotope calculations. We are indebted to editors Tom Marchitto and Ros Rickaby for feedback on the original manuscript. Ted McConnaughey, Vanni Aloisi and an anonymous reviewer provided constructive comments that helped clarify key points of the paper. We dedicate this work to Harry Elderfield for his pioneering contributions to the study of vital effects in biogenic carbonates and many fruitful conversations over the years about the lives of the small and calcareous.

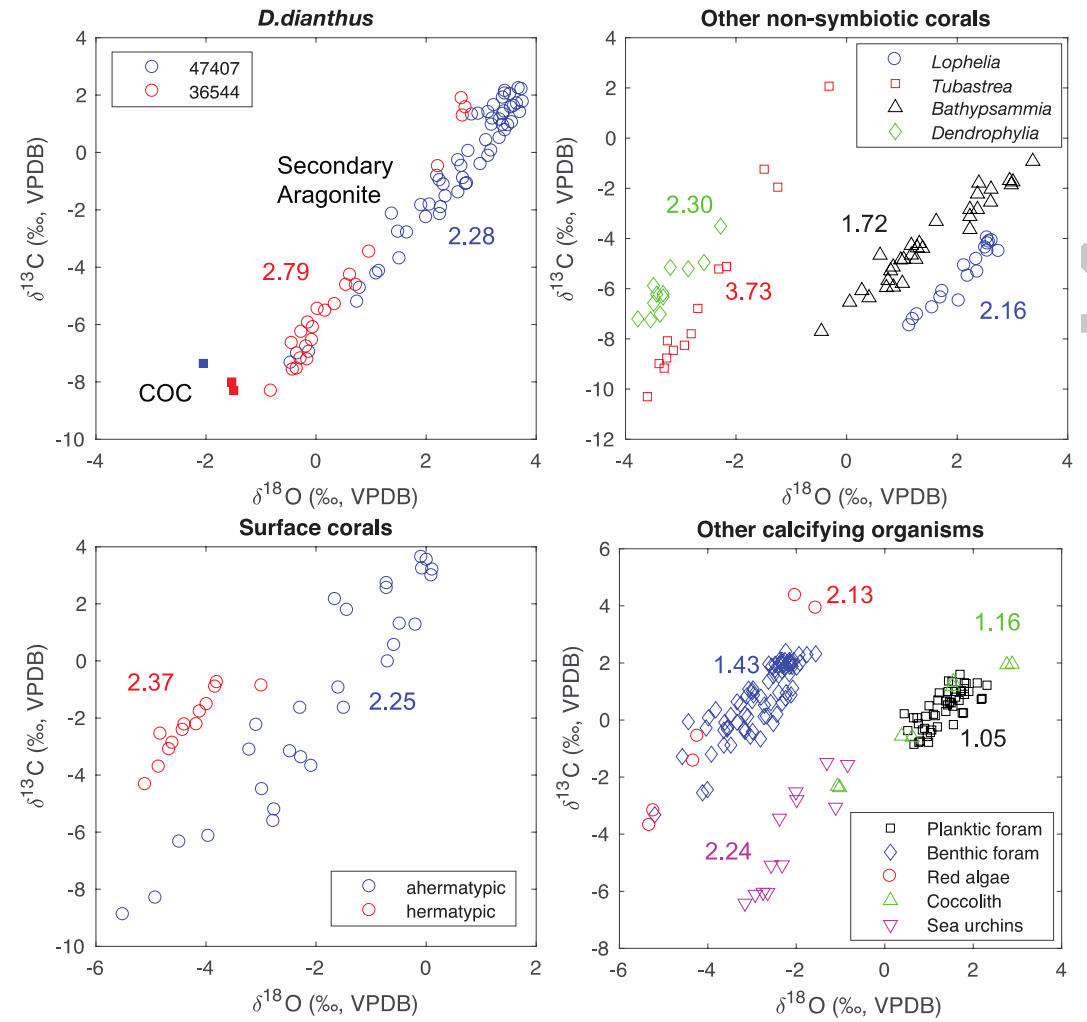

Figure 1 A compilation of stable isotope data in marine biogenic carbonates updated from McConnaughey (1989a). The labeled numbers are $\delta^{18}O$-$\delta^{13}C$ slopes of the corresponding dataset. (a) Two deep-sea coral *D.dianthus* specimens (Adkins et al., 2003). The squares are from COCs and are not included in the slope calculation. (b) Other non-symbiotic corals (Weber & Woodhead, 1970; Emiliani et al., 1978; McConnaughey, 1989a; Adkins et al., 2003). (c) Surface corals (Keith & Weber, 1965; Land & Lang, 1977). (d) Other calcifying organisms including planktic and benthic foraminifera (Vergnaud-Grazzini, 1976; Vinot-Bertouille & Duplessy, 1973), red algae (Keith & Weber, 1965), coccolithophores (Hermoso et al., 2014) and sea urchins (Weber & Raup, 1966). The difference in the intercepts of these datasets may result from temperature and metabolic CO_2 effects, and are not the focus of this study.

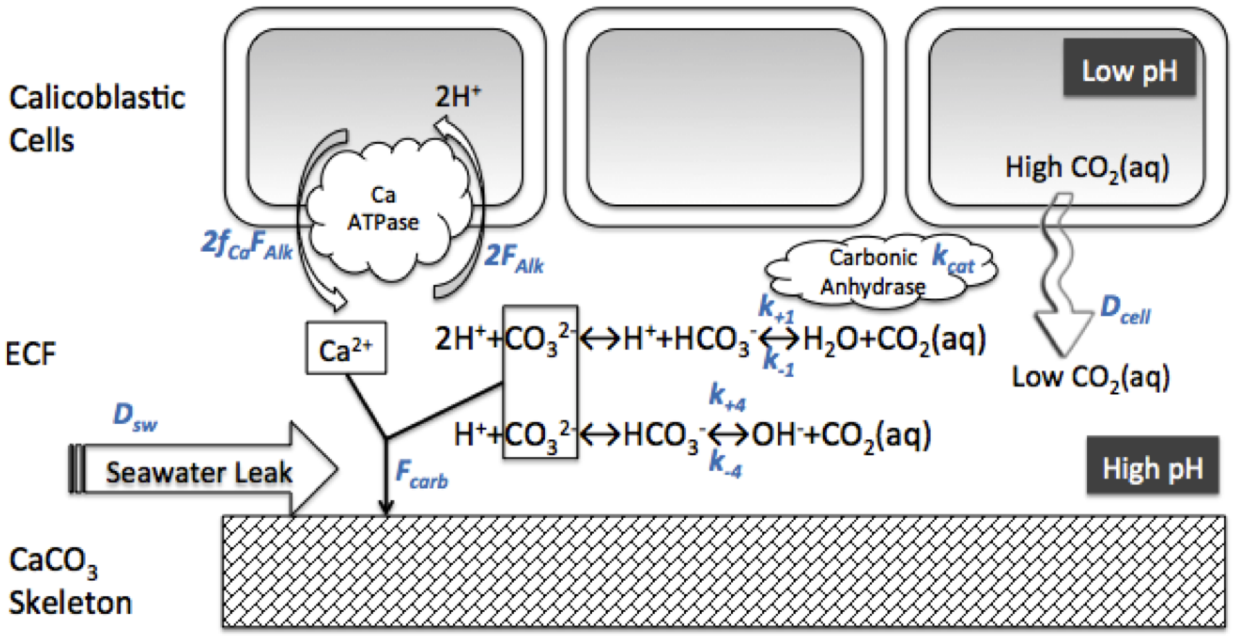

Figure 2 Schematic diagram of coral calcification. Black text shows the chemical species in the model, while blue text represents fluxes or reaction rate constants. The effect of carbonic anhydrase is represented by a rate enhancement factor k_{cat}. With carbonic anhydrase the rate constant for $CO_2(aq)$ hydration is $k_{cat} \cdot k_{+1}$ and HCO_3^- dehydration is $k_{cat} \cdot k_{-1}$. Conversion between HCO_3^- and CO_3^{2-} is considered instantaneous and the two are written together in the differential equations as equilibrated inorganic carbon (EIC) pool. The effect of Ca-APTase is represented by an exchange of Ca^{2+} into the ECF for two protons, which adds two units of alkalinity. The only DIC species that can passively move across the ECF membrane is $CO_2(aq)$, driven by the difference between $[CO_2(aq)]$ in the calicoblastic cells and $[CO_2(aq)]$ in the ECF.

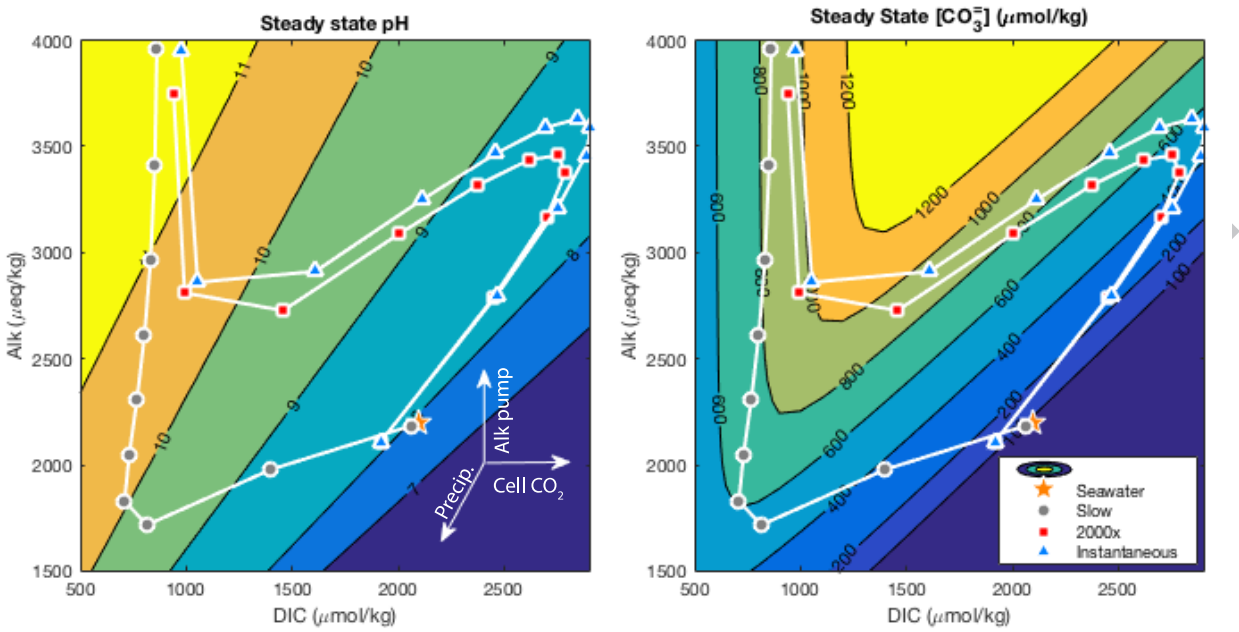

Figure 3 Steady state model solutions of DIC and alkalinity on pH and [CO_3^{2-}] contour plots for the slow kinetics (grey circles), instantaneous kinetics (blue triangles) and 2000× CA rate enhancement (red squares) cases. Each point represents a steady state solution to a given alkalinity pump rate. The pump rate increases along each path from the lower right corner to the upper left corner. The evolution paths are different for the slow kinetics case and the CA-enhanced case. The vectors represent the three major processes controlling the carbonate chemistry of the ECF in the model. The presence of CA increases the cell CO_2(aq) flux that generates higher DIC and buffers pH compared to the slow kinetics case.

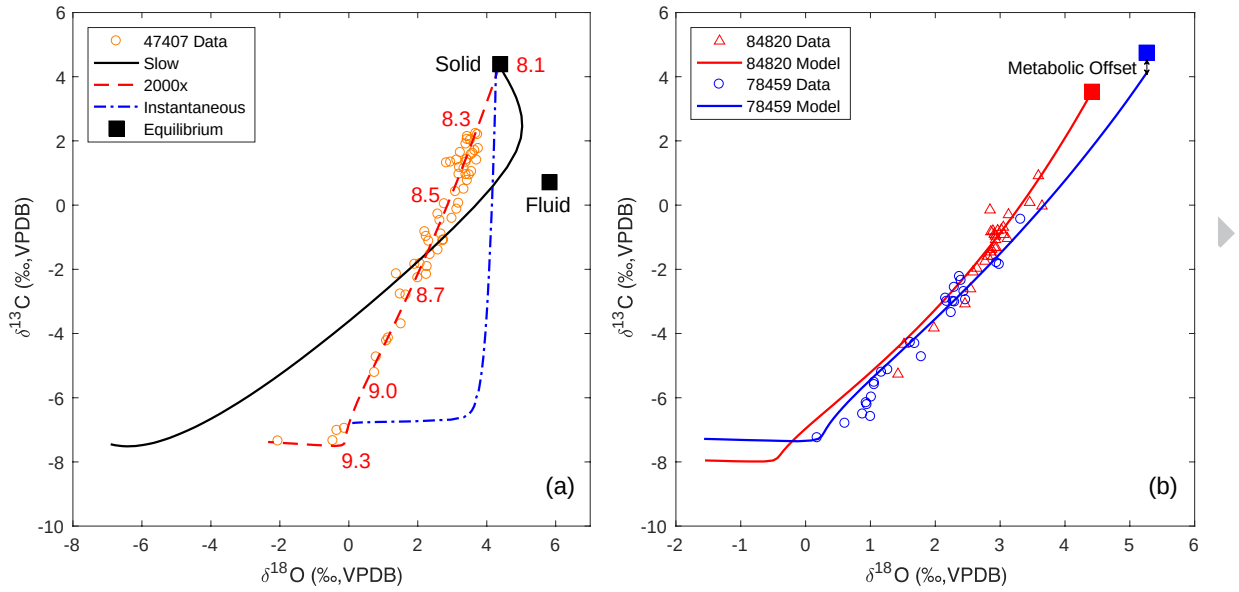

Figure 4 (a) Stable isotope composition of the coral skeleton from model output for the slow kinetics (black), instantaneous (blue) and 2000× CA rate enhancement (red) cases, compared to a deep-sea coral dataset (orange circles, Adkins et al., 2003). There is a systematic change in the slope of the $\delta^{18}O$-$\delta^{13}C$ trend with different CA activity. A 2000× CA rate enhancement generates a line that goes through the data. The model lines represent a series of steady state solutions with different alkalinity pump rates. An increase in pump rate drives the stable isotopes from the upper right corner (enriched values) to the lower left corner (depleted values). The black squares represent the steady state composition of the EIC and corresponding solid at zero pump rate. Isotope fractionation factors between the EIC and the solid carbonate based on inorganic experiments (Wang et al., 2013; Watkins et al., 2014; Watkins & Hunt, 2015) needs to be applied to make the model line go through the data. The red numbers mark the pH corresponding to the stable isotope compositions for the 2000× case. (b) Model fit to two other deep-sea corals (Adkins et al., 2003). The model lines are generated with all biological parameters the same as panel (a), including a 2000× CA rate enhancement, and varying only the ambient seawater conditions at each coral's collection site. A metabolic offset of 1‰ in $\delta^{13}C$ is applied to cross-membrane $CO_2(aq)$ (black arrow) to make the model line go through the data for coral 78459.

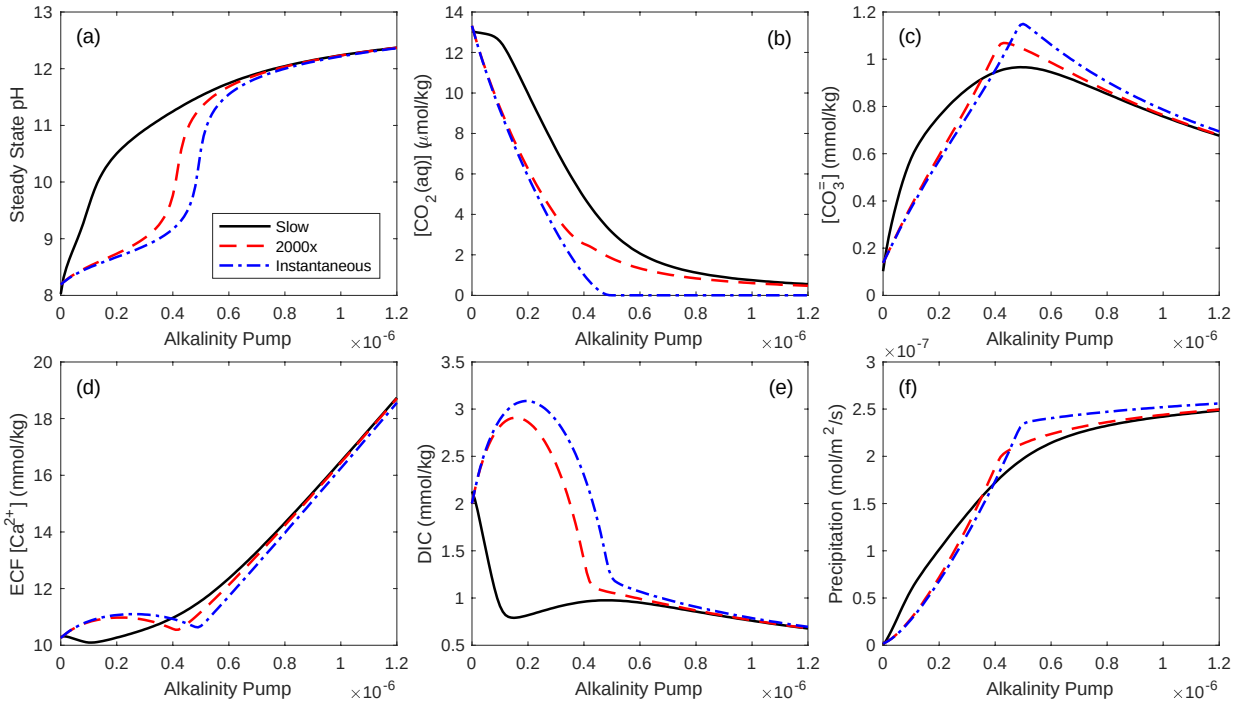

Figure 5 Steady state ECF carbonate chemistry as a function of the alkalinity pump strength (mol/m^2/s) for the slow kinetics (black), instantaneous kinetics (blue) and 2000× CA rate enhancement (red) cases. (a) The pH of the ECF is strongly buffered against the alkalinity pump with the presence of CA, up to a pH value of seawater pK_{a2} at 5°C (9.3). The pH of the slow kinetics case rises sharply at low pump rates. The model cases all converge when the pH is high enough for hydroxylation to be the dominant process in CO_2(aq)-EIC conversion. (b) With a kinetic barrier of CO_2(aq) hydration, the CO_2(aq) of the slow kinetics case pool in the ECF at low pump rates, and its rapid decrease lags the CA enhanced cases, until hydroxylation can convert it to EIC. (c) There is a maximum in [CO_3^{2-}] for all three cases, but the reasons for [CO_3^{2-}] increase are different. For the slow kinetics case, the [CO_3^{2-}] increase is caused by a sharp pH rise, while for the CA enhanced cases, the [CO_3^{2-}] increase is a combined result of DIC increase and pH rise. (d) The Ca^{2+} pumped into the ECF by Ca-ATPase is balanced by precipitation at low pump rates. At high pump rates, precipitation can no longer catch up with the pump, and [Ca^{2+}] increases rapidly. (e) CA concentrates DIC in the ECF relative to seawater over a range of alkalinity pump rates. (f) The precipitation rate increases with the pump rate, but there is a sharp change in the slope at the maximum [CO_3^{2-}] in (c) in all cases. Pumping alkalinity beyond the [CO_3^{2-}]$_{max}$ is energetically inefficient. Also the precipitation rate is more dependent on [CO_3^{2-}] than [Ca^{2+}], as has been previously suggested in laboratory simulation of biological calcification (Zeebe & Sanyal, 2002).

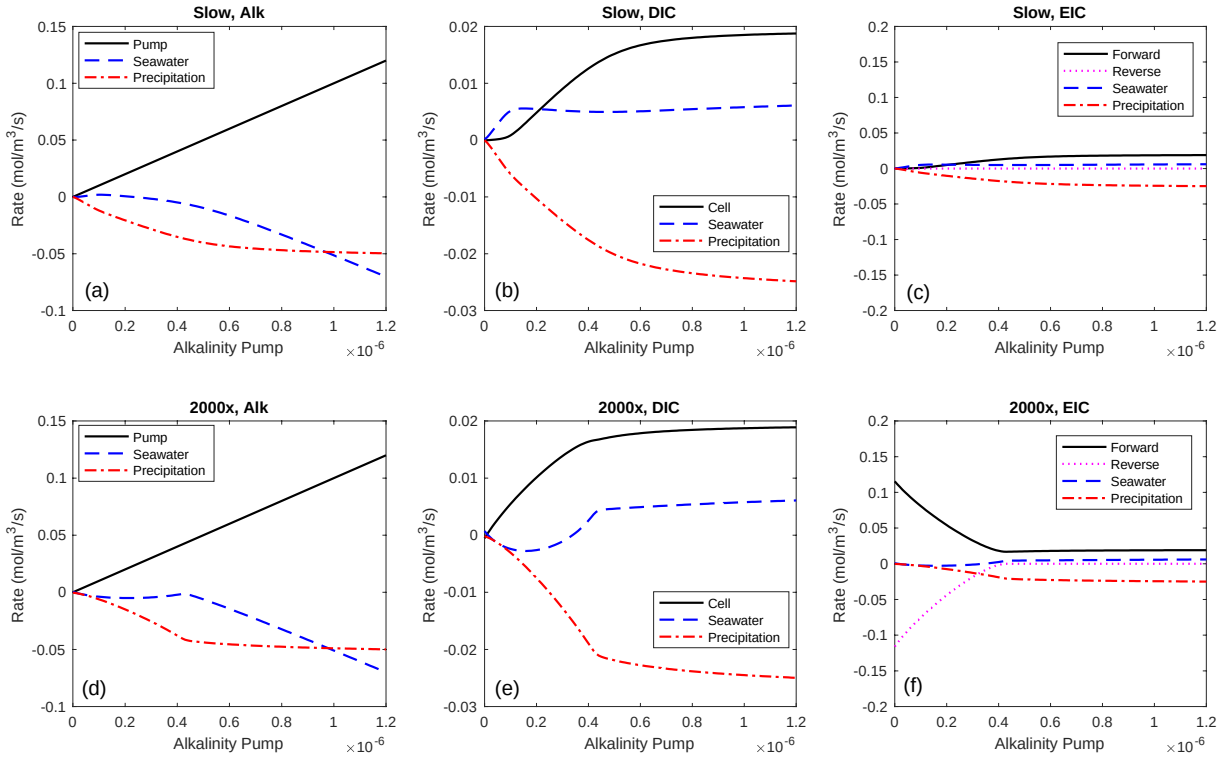

Figure 6 Flux balance at steady state for alkalinity, DIC and EIC at different pump rates. Panels (a)-(c) represents the slow kinetics case. Panels (d)-(f) represents the 2000× CA rate enhancement case. Seawater (blue dashed) and precipitation (red dot dashed) represent the tendency for ECF alkalinity, DIC and EIC to change with seawater transport and $CaCO_3$ precipitation. There is a source of alkalinity to the ECF by the Ca-ATPase pump (black solid in a and d), and a source of DIC from cross-membrane CO_2(aq) (black solid in b and e). EIC also feels the relative rates of the forward (hydration/hydroxylation, black solid in c and f) and reverse (dehydration/dehydroxylation, purple dotted in c and f) reactions of CO_2(aq)-EIC inter-conversion. The most apparent difference is the higher forward and reverse reaction rates for the 2000× case in the EIC fluxes. There is a larger imbalance between the forward and reverse reactions in the 2000× case that causes a low CO_2(aq) in the ECF. As a result, the gradient-driven cell CO_2(aq) flux increases more rapidly at low pump rates. This explains the DIC increase in Figure 5.

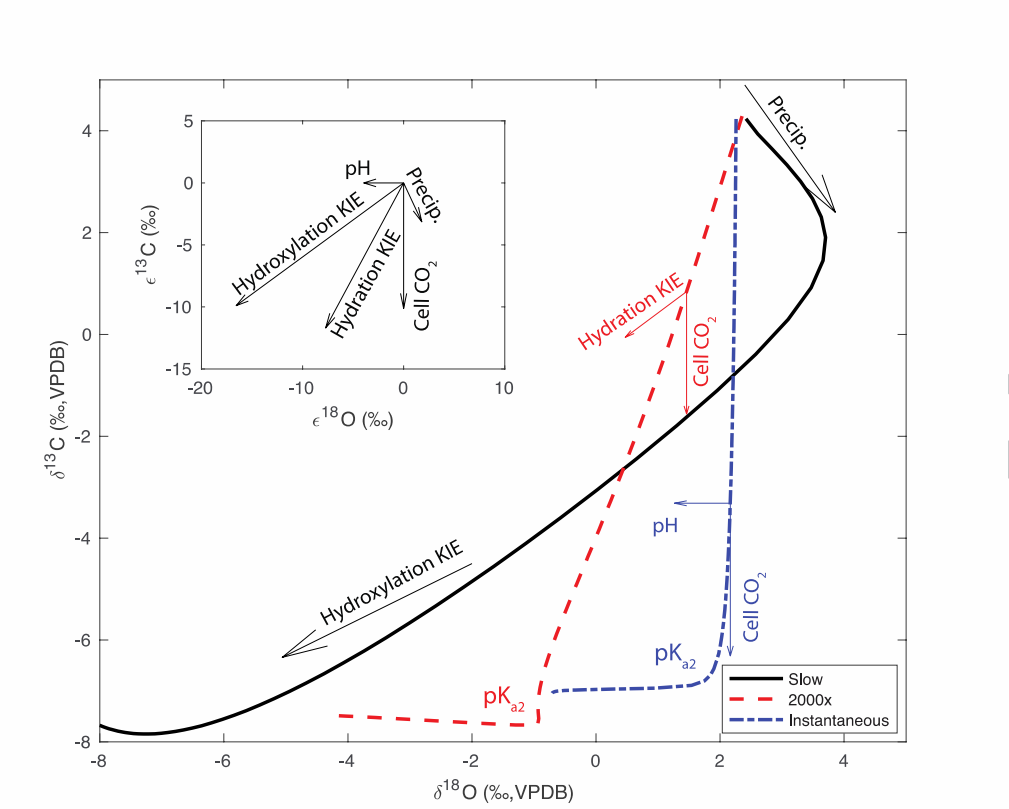

Figure 7 Decomposition of different isotope fractionation processes in the model results. The inset vector plot shows the isotope effects of five important processes in the model: pH-driven DIC speciation, input of cross-membrane CO_2(aq), hydration, hydroxylation and the Rayleigh effect by precipitation. The slow kinetics case shows two dominant processes at different ranges of pump rates. At low pump rates, a limited carbon supply from membrane crossing CO_2 creates the Rayleigh effect by precipitation. At high pump rates, high pH converts CO_2(aq) to HCO_3^- via the hydroxylation pathway and expresses the associated KIE. The presence of CA takes away the Rayleigh process by efficiently converting CO_2(aq) to HCO_3^- and providing a second source of carbon besides seawater. For instantaneous kinetics, the oxygen isotopes follow equilibrium DIC speciation, while the carbon fractionation is determined by the relative contribution of cell CO_2(aq) and seawater DIC. A maximum cell CO_2(aq) flux at pK_{a2} causes a kink in the correlation, and makes the slope too steep compared to the data. For a finite amount of CA such as the 2000× case, the hydration KIE is partly expressed. The amount of CA changes the timescale of DIC oxygen isotope equilibration, and determines how much hydration KIE is preserved in the skeleton, thus influencing the $\delta^{18}O$-$\delta^{13}C$ slope.

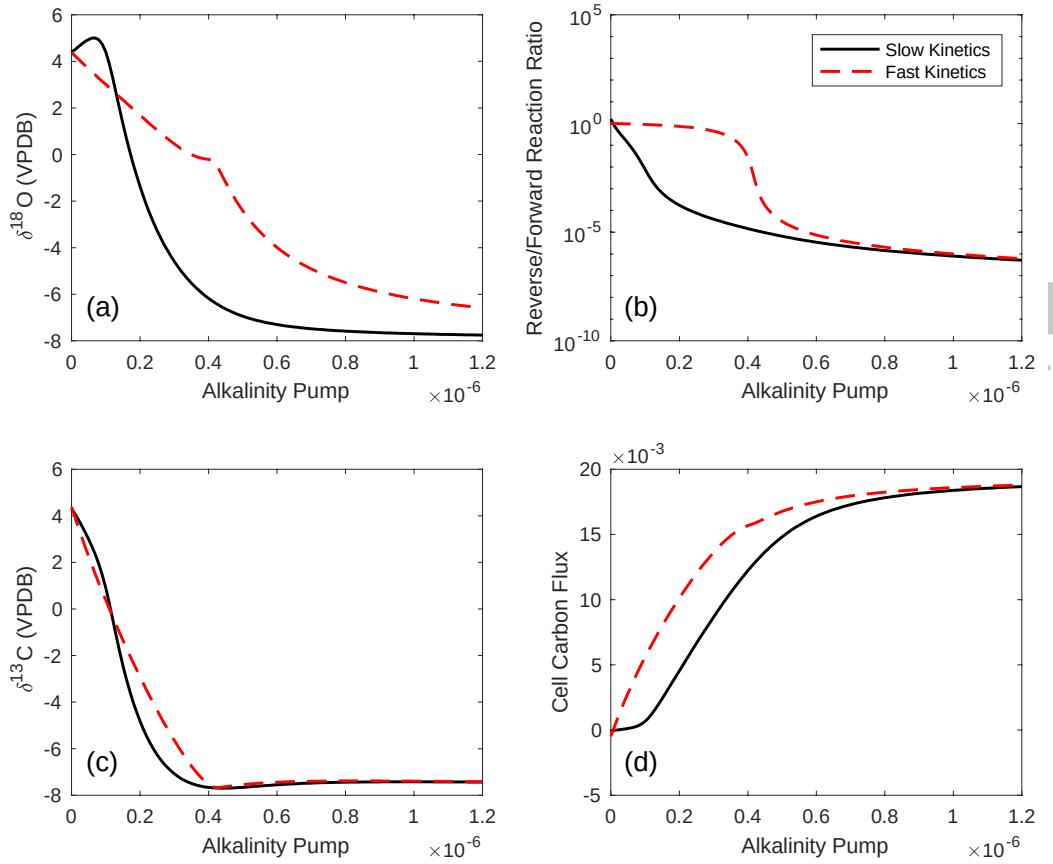

Figure 8 Processes that determine the isotope composition of the skeleton as a function of the alkalinity pump. The left column describes the isotope evolution of the skeleton for $\delta^{18}O$ and $\delta^{13}C$ respectively. The right column describes the main control on isotope compositions. (a-b) The range in $\delta^{18}O$ observed is mainly caused by KIEs during the CO_2(aq)-EIC inter-conversion. A measurement of the degree of oxygen isotope exchange is the ratio of reverse to forward reaction rates. A ratio of 1 represents equilibrium exchange, while smaller ratios cause stronger expression of KIEs. The presence of CA increases the exchange ratio for a given pump rate, and attenuates the $\delta^{18}O$ depletion by KIEs. (c-d) The observed $\delta^{13}C$ range is caused by the mixing of isotopically enriched seawater DIC and isotopically depleted cell CO_2(aq). As the alkalinity pump is turned up, more CO_2(aq) is converted to EIC, driving a larger cell CO_2(aq) flux. The cell CO_2(aq) is maximized beyond a threshold, causing a minimum in $\delta^{13}C$, and a kink in the $\delta^{18}O$-$\delta^{13}C$ relation.

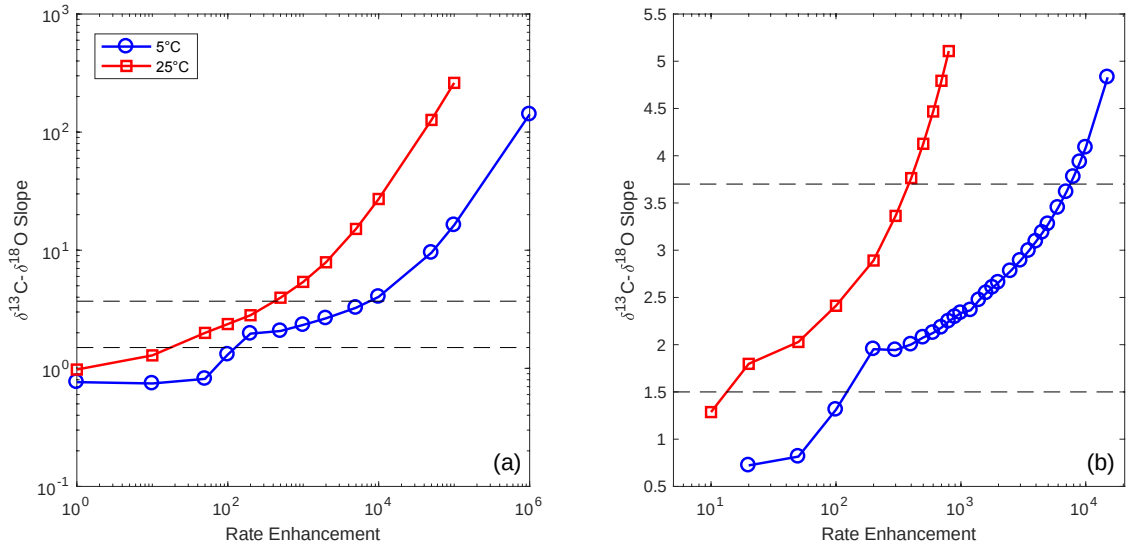

Figure 9 (a) The $\delta^{18}O$-$\delta^{13}C$ slope vs. CA rate enhancement factor (k_{cat}) for deep-sea coral (blue circles, 5°C) and surface ocean (red squares, 25°C) conditions. The dashed lines show the range of slopes (1.5-3.7) observed in different non-photosynthetic calcifying organisms. Panel (b) shows this range in more detail. In general, the slope increases with CA activity. The CA activity required for 25°C is lower than 5°C to have the same range of slopes. There is significant curvature in the $\delta^{18}O$-$\delta^{13}C$ plot at low CA activity that causes sharp turning points in these curves.

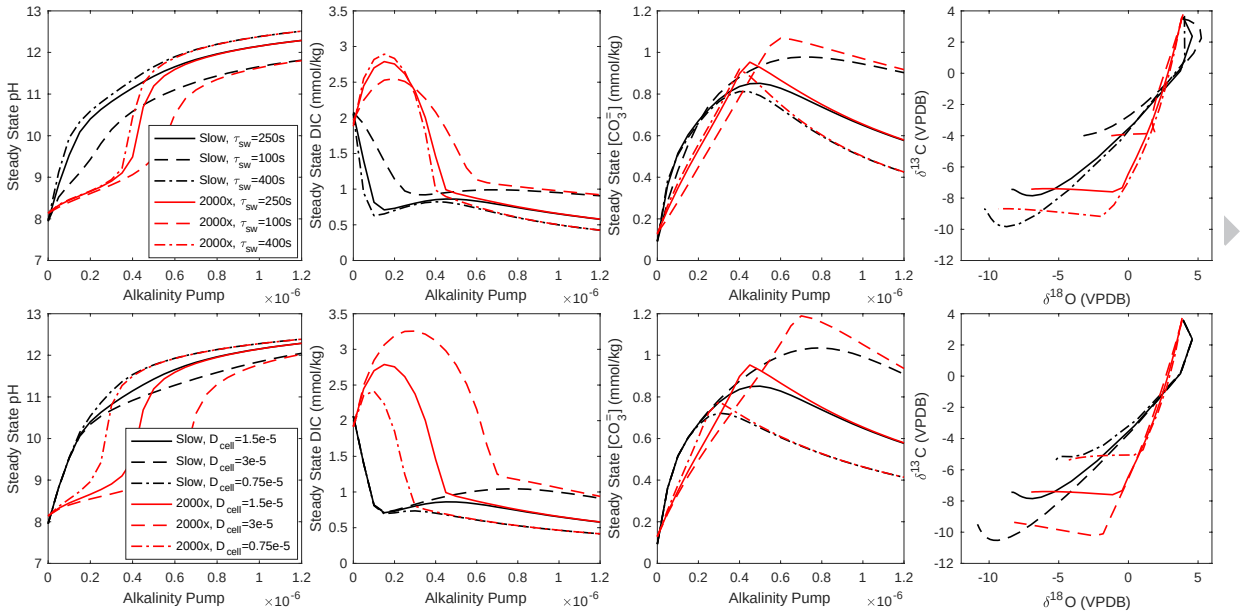

Figure 10 Model sensitivity to biological parameters. The top row shows the sensitivity of important variables to the seawater turnover timescale. The bottom row shows the sensitivity of the same variables to CO_2 diffusivity in cell membranes. The black curves show the slow kinetics case, while the red curves show the 2000× CA enhanced case. Faster seawater turnover or higher cell diffusivity makes the pH of the ECF more strongly buffered. In the parameter range explored, the differences in the shape of the pH, DIC and [CO_3^{2-}] curves remain for the slow kinetics and CA enhanced cases, showing the robustness of the model results. Changing the two parameters causes a change in the range of $\delta^{13}C$ in the model, but does not change the $\delta^{18}O$-$\delta^{13}C$ slope significantly. The $\delta^{18}O$-$\delta^{13}C$ kink is also a robust feature in the model, though the $\delta^{13}C$ value of the kink is a strong function of the balance of the seawater and cell carbon flux.

Appendix

Our model tracks the following chemical and isotope exchange reactions:

$$CO_2 + H_2O \overset{k_{+1}/k_{-1}}{\Longleftrightarrow} H^+ + HCO_3^-$$

$$CO_2 + OH^- \overset{k_{+4}/k_{-4}}{\Longleftrightarrow} HCO_3^-$$

$$^{13}CO_2 + H_2O \overset{k'_{+1}/k'_{-1}}{\Longleftrightarrow} H^+ + H^{13}CO_3^-$$

$$^{13}CO_2 + OH^- \overset{k'_{+4}/k'_{-4}}{\Longleftrightarrow} H^{13}CO_3^-$$

$$CO_2 + H_2^{18}O \overset{a_{+1}/a_{-1}}{\Longleftrightarrow} H^+ + HC^{18}OO_2^-$$

$$CO_2 + {}^{18}OH^- \overset{a_{+4}/a_{-4}}{\Longleftrightarrow} HC^{18}OO_2^-$$

$$C^{18}OO + H_2O \overset{b_{+1}/b_{-1}}{\Longleftrightarrow} H^+ + HC^{18}OO_2^-$$

$$C^{18}OO + OH^- \overset{b_{+4}/b_{-4}}{\Longleftrightarrow} HC^{18}OO_2^-$$

Following Zeebe & Wolf-Gladrow (2001), rate constants with subscripts +1 and -1 correspond to hydration and dehydration reactions, while subscripts +4 and -4 correspond hydroxylation and dehydroxylation reactions. Constants for ^{13}C substituted species are denoted as k'. Constants for ^{18}O substituted species are denoted 'a' or 'b', with 'a' representing substitution on H_2O or OH^-, and 'b' representing substitution on CO_2. The ratios for these rate constants are equal to the equilibrium constants of the reactions, and are listed in Appendix Table 1.

As shown in Figure 2, the model tracks the evolution of carbonate chemistry and the isotopically substituted species with time toward steady state. There are eight differential equations in the model as listed below:

$$(1)\ \frac{d[CO_2]}{dt} = -(k_{+1} + k_{+4}[OH^-])[CO_2] + (k_{-1}[H^+] + k_{-4})[EIC]\chi_1 + \frac{D_{cell}}{z}([CO_2]_{cell} - [CO_2]) + \frac{1}{\tau_{sw}}([CO_2]_{sw} - [CO_2])$$

$$(2)\ \frac{d[EIC]}{dt} = (k_{+1} + k_{+4}[OH^-])[CO_2] - (k_{-1}[H^+] + k_{-4})[EIC]\chi_1 + \frac{1}{\tau_{sw}}([EIC]_{sw} - [EIC]) - \frac{F_{CaCO_3}}{z}$$

$$(3)\ \frac{d[Alk]}{dt} = \frac{1}{\tau_{sw}}([Alk]_{sw} - [Alk]) + \frac{1}{z}(F_{Alk} - 2F_{CaCO_3})$$

$$(4)\ \frac{d[Ca^{2+}]}{dt} = \frac{1}{\tau_{sw}}([Ca^{2+}]_{sw} - [Ca^{2+}]) + \frac{1}{z}(\frac{1}{2}f_{Ca}F_{Alk} - F_{CaCO_3})$$

$$(5)\ \frac{d\left[{}^{13}CO_2\right]}{dt} = -(k'_{+1} + k'_{+4}[OH^-])\left[{}^{13}CO_2\right] + (k'_{-1}[H^+] + k'_{-4})\left[{}^{13}EIC\right]{}^{13}\chi_1 + \frac{D_{cell}}{z}\frac{1}{\alpha_{diff}}\left({}^{13}R_{CO_{2(cell)}}[CO_2]_{cell} - \left[{}^{13}CO_2\right]\right) + \frac{1}{\tau_{sw}}({}^{13}R_{CO_{2(sw)}}[CO_2]_{sw} - \left[{}^{13}CO_2\right])$$

$$(6)\ \frac{d\left[{}^{13}EIC\right]}{dt} = (k'_{+1} + k'_{+4}[OH^-])\left[{}^{13}CO_2\right] - (k'_{-1}[H^+] + k'_{-4})\left[{}^{13}EIC\right]{}^{13}\chi_1 + \frac{1}{\tau_{sw}}\left({}^{13}R_{EIC_{(sw)}}[EIC]_{sw} - \left[{}^{13}EIC\right]\right) - \frac{1}{z}F_{CaCO_3}\frac{\left[{}^{13}EIC\right]}{[EIC]}{}^{13}\alpha_{CaCO_3-EIC}$$

$$(7)\ \frac{d[C^{18}OO]}{dt} = -(b_{+1} + b_{+4}[OH^-])[C^{18}OO] + (b_{-1}[H^+] + b_{-4})\left[{}^{18}EIC\right]{}^{18}\chi_1 + \frac{D_{cell}}{z}\frac{1}{\alpha_{diff}}\left({}^{18}R_{CO_{2(cell)}}[CO_2]_{cell} - [C^{18}OO]\right) + \frac{1}{\tau_{sw}}({}^{18}R_{CO_{2(sw)}}[CO_2]_{sw} - [C^{18}OO])$$

$$(8)\ \frac{d\left[{}^{18}EIC\right]}{dt} = \frac{2}{3}(b_{+1} + b_{+4}[OH^-])[C^{18}OO] - \frac{2}{3}(b_{-1}[H^+] + b_{-4})\left[{}^{18}EIC\right]{}^{18}\chi_1 + \frac{1}{3}\left(a_{+1}{}^{18}R_{H_2O} + a_{+4}{}^{18}R_{OH}[OH^-]\right)[CO_2] - \frac{1}{3}(a_{-1}[H^+] + a_{-4})\left[{}^{18}EIC\right]{}^{18}\chi_1 + \frac{1}{\tau_{sw}}\left({}^{18}R_{EIC_{(sw)}}[EIC]_{sw} - \left[{}^{18}EIC\right]\right) - \frac{1}{z}F_{CaCO_3}\frac{\left[{}^{18}EIC\right]}{[EIC]}{}^{18}\alpha_{CaCO_3-EIC}$$

As discussed in the main text, we write HCO_3^- and CO_3^{2-} together as EIC, by assuming instantaneous equilibrium between these two species. The 2/3 and 1/3 factors in Eq. (8) represent the stoichiometric contribution of oxygen atoms to EIC from CO_2 and H_2O/OH^-, and are necessary to produce reasonable isotope compositions in the calculation. A similar formulation can be found in the appendix of Uchikawa & Zeebe (2012). Activity of carbonic anhydrase is implemented by multiplying k_{+1}, k_{-1}, k'_{+1}, k'_{-1}, a_{+1}, a_{-1}, b_{+1}, b_{-1} each with the rate enhancement factor k_{cat}, assuming no additional isotope effect from CA itself. The R's in the equations represent isotope ratios of EIC and CO_2(aq) from seawater and cell fluxes, and are calculated from equilibrium fractionation factors between the DIC species (Zhang et al., 1995; Beck et al., 2005; Wang et al., 2013). Definitions and values of the parameters and constants in the equations are listed in Appendix Table 1.

Appendix Table 1: Constants and parameters in the model

Part I Model Parameters			
Symbol	**Meaning**	**Value**	**Reference/Note**
z	ECF thickness	10 μm	Adkins et al., 2003; Gagnon et al., 2012
D_{cell}	Cell permeability of CO_2	0.0015 cm/s (variable)	Sultemeyer & Rinast, 1996
τ_{sw}	Seawater turnover timescale in ECF	230s (variable)	Tuned to fit data
$[CO_2]_{cell}$	Cell CO_2 concentration	13 μmol/kg	Adkins et al., 2003
F_{alk}	Alkalinity pump rate	0-1.2 μmol/m^2/s	Specified independent variable in model
f_{Ca}	Ca^{2+} fraction in Alk pump	0-1	Does not change basic model result
$[Alk]_{sw}$	Seawater alkalinity	2200 μmol/kg	Variable with corals
$[EIC]_{sw}/[CO_2]_{sw}$	Seawater EIC/CO_2(aq)	DIC=2000 μmol/kg	Calculated from Alk and DIC with CO2SYS, variable with corals
$[Ca]_{sw}$	Seawater Ca^{2+} concentration	10.3 mmol/kg	
Part II Physical Chemical Constants and Parameters			
Symbol	**Meaning**	**Value**	**Reference/Note**
F_{CaCO_3}	Aragonite precipitation flux (mol/m^2/s)	$F_{CaCO_3} = k_{rate}(\Omega - 1)^n$ $\Omega = \frac{[Ca^{2+}][CO_3^{2-}]}{K_{sp}}$ (Calculated by CO2SYS) $n = 1.7$ $\ln k_{rate} = 11.54 - \frac{8690}{T(K)}$	Romanek et al., 2011
k_{+1}	Rate constant of CO_2 hydration (s^{-1})	$\ln k_{+1} = 1246.98 - \frac{61900}{T(K)} - 183.0 \ln T(K)$	Johnson (1982)
k_{-1}	Rate constant of HCO_3^- dehydration ($M^{-1}\cdot s^{-1}$)	$k_{-1} = k_{+1}/K_{a1}$	K_{a1} from CO2SYS
k_{+4}	Rate constant of CO_2 hydroxylation ($M^{-1}\cdot s^{-1}$)	$\ln k_{+4} = 17.67 - \frac{2790.47}{T(K)}$	Johnson (1982); Zeebe & Wolf-Gladrow (2001)
k_{-4}	Rate constant of HCO_3^- dehydroxylation (s^{-1})	$k_{-4} = k_{+4}\frac{K_w}{K_{a1}}$	K_{a1} and K_w from CO2SYS
χ_1	Fraction of HCO_3^- in EIC	$\chi_1 = \frac{1}{1 + \frac{K_{a2}}{[H^+]}}$	K_{a2} from CO2SYS
Part III Isotope Related Parameters and Fractionation Factors			
Symbol	**Meaning**	**Value**	**Reference/Note**
α_{diff}	Fractionation factor of	1.0007	O'Leary, 1984

	CO_2 diffusion across membrane		Assumed the same for ^{13}C and ^{18}O
$^{13}\chi_1$	Fraction of $H^{13}CO_3^-$ in ^{13}EIC	$^{13}\chi_1 = \frac{1}{1 + \frac{K_{a2} \cdot {}^{13}\alpha_{CO_3-HCO_3}}{[H^+]}}$	
$^{18}\chi_1$	Fraction of $HC^{18}OO_2^-$ in ^{18}EIC	$^{18}\chi_1 = \frac{1}{1 + \frac{K_{a2} \cdot {}^{18}\alpha_{CO_3-HCO_3}}{[H^+]}}$	
k'_{+1}	Rate constant for $^{13}CO_2$ hydration (s^{-1})	$k_{+1}/k'_{+1} = 1.0013$	O'Leary et al, 1992
k'_{-1}	Rate constant for $H^{13}CO_3^-$ dehydration ($M^{-1}\cdot s^{-1}$)	$k'_{+1}/k'_{-1} = K_{a1} \cdot {}^{13}\alpha_{HCO_3-CO_2(aq)}$	Calculated from k'_{+1} and $^{13}\alpha_{HCO_3-CO_2(aq)}$
k'_{+4}	Rate constant for $^{13}CO_2$ hydroxylation (s^{-1})	$k_{+4}/k'_{+4} = 1.0011$	Zeebe et al., 1999b; Zeebe & Wolf-Gladrow, 2001
k'_{-4}	Rate constant for $H^{13}CO_3^-$ dehydroxylation ($M^{-1}\cdot s^{-1}$)	$k'_{+4}/k'_{-4} = \frac{K_{a1}}{K_w} \cdot {}^{13}\alpha_{HCO_3-CO_2(aq)}$	Calculated from k'_{+4} and $^{13}\alpha_{HCO_3-CO_2(aq)}$
a_{+1}, b_{+1}	Rate constants for hydration with ^{18}O species (s^{-1})	$k_{+1}/a_{+1} = 1.007$ $k_{+1}/b_{+1} = 1.010$ When k_{cat}=2000	Zeebe, 2014 A range of values can fit data, and fit depends on k_{cat}
a_{-1}, b_{-1}	Rate constants for dehydration with ^{18}O species ($M^{-1}\cdot s^{-1}$)	$a_{+1}/a_{-1} = K_{a1} \cdot {}^{18}\alpha_{HCO_3-H_2O}$ $b_{+1}/b_{-1} = K_{a1} \cdot {}^{18}\alpha_{HCO_3-CO_2}$	Calculated from a_{+1}, b_{+1}, $^{18}\alpha_{HCO_3-H_2O}$, $^{18}\alpha_{HCO_3-CO_2}$
a_{+4}, b_{+4}	Rate constants for hydroxylation with ^{18}O species ($M^{-1}\cdot s^{-1}$)	Assumed the same as a_{+1}, b_{+1}	No constraint available, does not influence $\delta^{18}O$-$\delta^{13}C$ slope, and only changes isotope values after the kink
a_{-4}, b_{-4}	Rate constants for dehydroxylation with ^{18}O species (s^{-1})	$a_{+4}/a_{-4} = \frac{K_{a1}}{K_w} \cdot \frac{{}^{18}\alpha_{HCO_3-H_2O}}{{}^{18}\alpha_{OH-H_2O}}$ $b_{+4}/b_{-4} = \frac{K_{a1}}{K_w} \cdot {}^{18}\alpha_{HCO_3-CO_2}$	Calculated from a_{+4}, b_{+4} and the corresponding equilibrium fractionation factors
$^{13}\alpha_{DIC-CO_2(g)}$	^{13}C fractionation between DIC species and CO_2(g)	Temperature dependent	Zhang et al., 1995
$^{18}\alpha_{DIC-H_2O(g)}$	^{18}O fractionation between DIC species and H_2O	Temperature dependent	Wang et al., 2013
$^{18}\alpha_{OH-H_2O(g)}$	^{18}O fractionation between OH^- and H_2O	Temperature dependent	Wang et al., 2013
$^{13}\alpha_{CaCO_3-EIC}$, $^{18}\alpha_{CaCO_3-EIC}$	^{13}C and ^{18}O fractionation between solid carbonate and EIC	Temperature, pH and growth rate dependent	Wang et al., 2013; Watkins et al., 2014; Watkins & Hunt, 2015

References

Addadi, L., Raz, S., & Weiner, S. (2003). Taking Advantage of Disorder: Amorphous Calcium Carbonate and Its Roles in Biomineralization. *Advanced Materials, 15*(12), 959-970. doi: 10.1002/adma.200300381

Adkins, J. F., Boyle, E. A., Curry, W. B., & Lutringer, A. (2003). Stable isotopes in deep-sea corals and a new mechanism for "vital effects". *Geochimica et Cosmochimca Acta, 67*, 1129-1143.

Adkins, J. F., Griffin, S., Kashgarian, M., Cheng, H., Druffel, E. R. M., Boyle, E. A., Edwards, R.L., Shen, C.-C. (2002). Radiocarbon dating of deep-sea corals. *Radiocarbon, 44*, 567-580.

Al-Horani, F. A., Al-Moghrabi, S. M., & de Beer, D. (2003). The mechanism of calcification and its relation to photosynthesis and respiration in the scleractinian coral Galaxea fascicularis. *Marine Biology, 142*(3), 419-426. doi: 10.1007/s00227-002-0981-8

Allison, N., Cohen, I., Finch, A. A., Erez, J., & Tudhope, A. W. (2014). Corals concentrate dissolved inorganic carbon to facilitate calcification. *Nature Communications, 5*, 5741. doi: 10.1038/ncomms6741

Beck, W. C., Grossman, E. L., & Morse, J. W. (2005). Experimental studies of oxygen isotope fractionation in the carbonic acid system at 15°, 25°, and 40°C. *Geochimica et Cosmochimca Acta, 69*, 3493-3503.

Bertucci, A., Tambutté, S., Supuran, C. T., Allemand, D., & Zoccola, D. (2011). A New Coral Carbonic Anhydrase in Stylophora pistillata. *Marine Biotechnology, 13*(5), 992-1002. doi: 10.1007/s10126-011-9363-x

Bertucci, A., Zoccola, D., Tambutté, S., Vullo, D., & Supuran, C. T. (2010). Carbonic anhydrase activators. The first activation study of a coral secretory isoform with amino acids and amines. *Bioorganic & Medicinal Chemistry, 18*(6), 2300-2303. doi: https://doi.org/10.1016/j.bmc.2010.01.059

Blamart, D., Rollion-Bard, C., Meibom, A., Cuif, J. P., Juillet-Leclerc, A., & Dauphin, Y. (2007). Correlation of boron isotopic composition with ultrastructure in the deep-sea coral Lophelia pertusa: Implications for biomineralization and paleo-pH. *Geochemistry, Geophysics, Geosystems, 8*(12). doi: 10.1029/2007GC001686

Cai, W.-J., Ma, Y., Hopkinson, B. M., Grottoli, A. G., Warner, M. E., Ding, Q., Hu, X., Yuan, X., Schoepf,.V., Xu, H., Han, C., Melman, T.F., Hoadley, K.D., Pettay, D.T., Matsui, Y., Baumann, J.H., Levas, S., Ying, Y., & Wang, Y. (2016). Microelectrode characterization of coral daytime interior pH and carbonate chemistry. *Nature Communications, 7*, 11144. doi: 10.1038/ncomms11144

Case, D. H., Robinson, L. F., Auro, M. E., & Gagnon, A. C. (2010). Environmental and biological controls on Mg and Li in deep-sea scleractinian corals. *Earth and Planetary Science Letters, 300*(3–4), 215-225. doi: http://dx.doi.org/10.1016/j.epsl.2010.09.029

Cuif, J.-P., & Dauphin, Y. (2005). The two-step mode of growth in the scleractinian coral skeletons from the micrometre to the overall scale. *Journal of Structural Biology, 150*(3), 319-331. doi: https://doi.org/10.1016/j.jsb.2005.03.004

De Yoreo, J. J., Wierzbicki, A., & Dove, P. M. (2007). New insights into mechanisms of biomolecular control on growth of inorganic crystals. *CrystEngComm, 9*(12), 1144-1152. doi: 10.1039/B713006F

Demény, A., Németh, P., Czuppon, G., Leél-Őssy, S., Szabó, M., Judik, K., Németh, T., Stieber, J. (2016). Formation of amorphous calcium carbonate in caves and its implications for speleothem research. *Scientific Reports, 6*, 39602. doi: 10.1038/srep39602

Emiliani, C., Hudson, J. H., Shinn, E. A., & George, R. Y. (1978). Oxygen and Carbon Isotopic Growth

Record in a Reef Coral from the Florida Keys and a Deep-Sea Coral from Blake Plateau. *Science, 202*(4368), 627.

Gabitov, R. I. (2013). Growth-rate induced disequilibrium of oxygen isotopes in aragonite: An in situ study. *Chemical Geology, 351*, 268-275. doi: https://doi.org/10.1016/j.chemgeo.2013.05.015

Gabitov, R. I., Watson, E. B., & Sadekov, A. (2012). Oxygen isotope fractionation between calcite and fluid as a function of growth rate and temperature: An in situ study. *Chemical Geology, 306–307*, 92-102. doi: https://doi.org/10.1016/j.chemgeo.2012.02.021

Gagnon, A. C., Adkins, J. F., Fernandez, D. P., & Robinson, L. F. (2007). Sr/Ca and Mg/Ca vital effects correlated with skeletal architecture in a scleractinian deep-sea coral and the role of Rayleigh fractionation. *Earth and Planetary Science Letters, 261*, 280–295.

Gagnon, A. C., Adkins, J. F., & Erez, J. (2012). Seawater transport during coral biomineralization. *Earth and Planetary Science Letters, 329–330*, 150-161. doi: http://dx.doi.org/10.1016/j.epsl.2012.03.005

Gago-Duport, L., Briones, M. J. I., Rodríguez, J. B., & Covelo, B. (2008). Amorphous calcium carbonate biomineralization in the earthworm's calciferous gland: Pathways to the formation of crystalline phases. *Journal of Structural Biology, 162*(3), 422-435. doi: https://doi.org/10.1016/j.jsb.2008.02.007

Gladfelter, E. H. (1982). Skeletal development in *Acropora cervicornis*: I. Patterns of calcium carbonate accretion in the axial corallite. *Coral Reefs, 1*(1), 45-51. doi: 10.1007/BF00286539

Gong, Y. U. T., Killian, C. E., Olson, I. C., Appathurai, N. P., Amasino, A. L., Martin, M. C., Holt, L.J., Wilt, F.H., & Gilbert, P. U. P. A. (2012). Phase transitions in biogenic amorphous calcium carbonate. *Proceedings of the National Academy of Sciences, 109*(16), 6088-6093.

Goreau, T. F. (1959). Thy physiology of skeleton formation in corals. I. A method for measuring the rate of calcium deposition by corals under different conditions. *The Biological Bulletin, 116*(1), 59-75. doi: 10.2307/1539156

Hentunen, T. A., Härkönen, P. L., & Väänänen, H. K. (2000). Carbonic anhydrases in calcified tissues. In W. R. Chegwidden, N. D. Carter & Y. H. Edwards (Eds.), *The Carbonic Anhydrases: New Horizons* (pp. 491-497). Basel: Birkhäuser Basel.

Hermoso, M., Horner, T. J., Minoletti, F., & Rickaby, R. E. M. (2014). Constraints on the vital effect in coccolithophore and dinoflagellate calcite by oxygen isotopic modification of seawater. *Geochimica et Cosmochimica Acta, 141*, 612-627. doi: http://dx.doi.org/10.1016/j.gca.2014.05.002

Hermoso, M., Minoletti, F., Aloisi, G., Bonifacie, M., McClelland, H. L. O., Labourdette, N., . . . Rickaby, R. E. M. (2016). An explanation for the 18O excess in Noelaerhabdaceae coccolith calcite. *Geochimica et Cosmochimica Acta, 189*(Supplement C), 132-142. doi: https://doi.org/10.1016/j.gca.2016.06.016

Hopkinson, B. M., Tansik, A. L., & Fitt, W. K. (2015). Internal carbonic anhydrase activity in the tissue of scleractinian corals is sufficient to support proposed roles in photosynthesis and calcification. *The Journal of Experimental Biology, 218*(13), 2039.

Jacob, D. E., Soldati, A. L., Wirth, R., Huth, J., Wehrmeister, U., & Hofmeister, W. (2008). Nanostructure, composition and mechanisms of bivalve shell growth. *Geochimica et Cosmochimica Acta, 72*(22), 5401-5415. doi: https://doi.org/10.1016/j.gca.2008.08.019

Johnson, K. S. (1982). Carbon dioxide hydration and dehydration kinetics in seawater. *Limnology and Oceanography, 27*(5), 849-855. doi: 10.4319/lo.1982.27.5.0849

Juillet-Leclerc, A., & Reynaud, S. (2010). Light effects on the isotopic fractionation of skeletal oxygen and carbon in the cultured zooxanthellate coral, *Acropora*: implications for coral-growth rates.

Biogeosciences, 7(3), 893-906. doi: 10.5194/bg-7-893-2010

Keith, M. L., & Weber, J. N. (1965). Systematic Relationships between Carbon and Oxygen Isotopes in Carbonates Deposited by Modern Corals and Algae. *Science, 150*(3695), 498.

Kim, S.-T., & O'Neil, J. R. (1997). Temperature dependence of $\delta^{18}O$. *Geochemica et Cosmochimica Acta, 61*, 3461-3475.

Land, L. S., Lang, J. C., & Barnes, D. J. (1977). On the stable carbon and oxygen isotopic composition of some shallow water, ahermatypic, scleractinian coral skeletons. *Geochimica et Cosmochimica Acta, 41*, 169-172.

Marlier, J. F., & O'Leary, M. H. (1984). Carbon kinetic isotope effects on the hydration of carbon dioxide and the dehydration of bicarbonate ion. *Journal of the American Chemical Society, 106*(18), 5054-5057. doi: 10.1021/ja00330a003

Mass, T., Drake, J. L., Peters, E. C., Jiang, W., & Falkowski, P. G. (2014). Immunolocalization of skeletal matrix proteins in tissue and mineral of the coral Stylophora pistillata. *Proceedings of the National Academy of Sciences, 111*(35), 12728-12733.

McConnaughey, T. A. (1989a). ^{13}C and ^{18}O isotopic disequilibrium in biological carbonates: I. Patterns. *Geochimica et Cosmochimica Acta, 53*, 151-162.

McConnaughey, T. A. (1989b). ^{13}C and ^{18}O isotopic disequilibrium in biological carbonates: II. In vitro simulation of kinetic isotope effects. *Geochim. Cosmochim. Acta, 53*, 163-171.

McCrea, J. M. (1950). On the isotopic chemistry of carbonates and a paleotemperature scale. *Journal of Chemical Physics, 18*, 849-857.

McCulloch, M., Trotter, J., Montagna, P., Falter, J., Dunbar, R., Freiwald, A., Försterra, G., López Correa, M., Maier, C., Rüggeberg, A., & Taviani, M. (2012). Resilience of cold-water scleractinian corals to ocean acidification: Boron isotopic systematics of pH and saturation state up-regulation. *Geochimica et Cosmochimica Acta, 87*, 21-34. doi: https://doi.org/10.1016/j.gca.2012.03.027

Moya, A., Tambutté, S., Bertucci, A., Tambutté, E., Lotto, S., Vullo, D., Supuran, C.T., Allemand, D., & Zoccola, D. (2008). Carbonic Anhydrase in the Scleractinian Coral Stylophora pistillata: characterization, localization, and role in biomineralization. *Journal of Biological Chemistry, 283*(37), 25475-25484.

O'Leary, M. H. (1984). Measurement of the isotope fractionation associated with diffusion of carbon dioxide in aqueous solution. *The Journal of Physical Chemistry, 88*(4), 823-825. doi: 10.1021/j150648a041

O'Leary, M. H., Madhavan, S., & Paneth, P. (1992). Physical and chemical basis of carbon isotope fractionation in plants. *Plant, Cell & Environment, 15*(9), 1099-1104. doi: 10.1111/j.1365-3040.1992.tb01660.x

Robinson, L. F., Adkins, J. F., Fernandez, D. P., Burnett, D. S., Wang, S. L., Gagnon, A. C., & Krakauer, N. (2006). Primary U distribution in scleractinian corals and its implications for U series dating. *Geochemistry, Geophysics, Geosystems, 7*, Q05022. doi: 10.1029/2005GC001138

Rollion-Bard, C., Blamart, D., Cuif, J.-P., & Dauphin, Y. (2010). In situ measurements of oxygen isotopic composition in deep-sea coral, Lophelia pertusa: Re-examination of the current geochemical models of biomineralization. *Geochimica et Cosmochimica Acta, 74*(4), 1338-1349. doi: https://doi.org/10.1016/j.gca.2009.11.011

Rollion-Bard, C., Chaussidon, M., & France-Lanord, C. (2003). pH control on oxygen isotopic composition of symbiotic corals. *Earth and Planetary Science Letters, 215*, 275-288.

Romanek, C. S., Grossman, E. L., & Morse, J. W. (1992). Carbon isotopic fractionation in synthetic aragonite and calcite: Effects of temperature and precipitation rate. *Geochimica et Cosmochimica*

Acta, *56*(1), 419-430. doi: http://dx.doi.org/10.1016/0016-7037(92)90142-6

Romanek, C. S., Morse, J. W., & Grossman, E. L. (2011). Aragonite Kinetics in Dilute Solutions. *Aquatic Geochemistry*, *17*(4), 339. doi: 10.1007/s10498-011-9127-2

Spero, H. J., Bijma, J., Lea, D. W., & Bemis, B. E. (1997). Effect of seawater carbonate concentration on foraminiferal carbon and oxygen isotopes. *Nature*, *390*, 497-500.

Sültemeyer, D., & Rinast, K.-A. (1996). The CO_2 permeability of the plasma membrane of Chlamydomonas reinhardtii: mass-spectrometric ^{18}O-exchange measurements from $^{13}C^{18}O_2$ in suspensions of carbonic anhydrase-loaded plasma-membrane vesicles. *Planta*, *200*(3), 358-368. doi: 10.1007/BF00200304

Tambutté, S., Tambutté, E., Zoccola, D., Caminiti, N., Lotto, S., Moya, A., Allemand, D., & Adkins, J. (2007). Characterization and role of carbonic anhydrase in the calcification process of the azooxanthellate coral Tubastrea aurea. *Marine Biology*, *151*(1), 71-83. doi: 10.1007/s00227-006-0452-8

Tambutté, S., Holcomb, M., Ferrier-Pagès, C., Reynaud, S., Tambutté, É., Zoccola, D., & Allemand, D. (2011). Coral biomineralization: From the gene to the environment. *Journal of Experimental Marine Biology and Ecology*, *408*(1–2), 58-78. doi: http://dx.doi.org/10.1016/j.jembe.2011.07.026

Tambutté, E., Tambutté, S., Segonds, N., Zoccola, D., Venn, A., Erez, J., & Allemand, D. (2012). Calcein labelling and electrophysiology: insights on coral tissue permeability and calcification. *Proceedings of the Royal Society B: Biological Sciences*, *279*(1726), 19.

Uchikawa, J., & Zeebe, R. E. (2012). The effect of carbonic anhydrase on the kinetics and equilibrium of the oxygen isotope exchange in the CO_2–H_2O system: Implications for $\delta^{18}O$ vital effects in biogenic carbonates. *Geochimica et Cosmochimica Acta*, *95*, 15-34. doi: http://dx.doi.org/10.1016/j.gca.2012.07.022

Urey, H. C. (1947). The thermodynamic properties of isotopic substances. *J. Chem. Soc.*, *1947*, 562-581.

Usdowski, E., & Hoefs, J. (1993). Oxygen isotope exchange between carbonic acid, bicarbonate, and water: a re-examination of the data of McCrea (1950) and an expression for the overall partitioning of oxygen isotopes between the carbonate species and water. *Geochimica et Cosmochimica Acta*, *57*, 3815-3818.

Venn, A., Tambutté, E., Holcomb, M., Allemand, D., & Tambutté, S. (2011). Live Tissue Imaging Shows Reef Corals Elevate pH under Their Calcifying Tissue Relative to Seawater. *PLOS ONE*, *6*(5), e20013. doi: 10.1371/journal.pone.0020013

Vergnaud Grazzini, C. (1976). Non-equilibrium isotopic compositions of shells of planktonic foraminifera in the Mediterranean sea. *Palaeogeography, Palaeoclimatology, Palaeoecology*, *20*(4), 263-276. doi: http://dx.doi.org/10.1016/0031-0182(76)90007-9

Vinot-Bertouille, A.-C., & Duplessy, J.-C. (1973). Individual isotopic fractionation of carbon and oxygen in benthic foraminifera. *Earth and Planetary Science Letters*, *18*(2), 247-252. doi: http://dx.doi.org/10.1016/0012-821X(73)90063-0

Von Euw, S., Zhang, Q., Manichev, V., Murali, N., Gross, J., Feldman, L. C., Gustafsson, T., Flach, C., Mendelsohn, R., & Falkowski, P. G. (2017). Biological control of aragonite formation in stony corals. *Science*, *356*(6341), 933.

Wall, M., Ragazzola, F., Foster, L. C., Form, A., & Schmidt, D. N. (2015). pH up-regulation as a potential mechanism for the cold-water coral *Lophelia pertusa* to sustain growth in aragonite undersaturated conditions. *Biogeosciences*, *12*(23), 6869-6880. doi: 10.5194/bg-12-6869-2015

Wang, Z., Gaetani, G., Liu, C., & Cohen, A. (2013). Oxygen isotope fractionation between aragonite and seawater: Developing a novel kinetic oxygen isotope fractionation model. *Geochimica et*

Cosmochimica Acta, 117, 232-251. doi: https://doi.org/10.1016/j.gca.2013.04.025

Watkins, J. M., & Hunt, J. D. (2015). A process-based model for non-equilibrium clumped isotope effects in carbonates. *Earth and Planetary Science Letters, 432*, 152-165. doi: https://doi.org/10.1016/j.epsl.2015.09.042

Watkins, J. M., Hunt, J. D., Ryerson, F. J., & DePaolo, D. J. (2014). The influence of temperature, pH, and growth rate on the $\delta^{18}O$ composition of inorganically precipitated calcite. *Earth and Planetary Science Letters, 404*, 332-343. doi: http://dx.doi.org/10.1016/j.epsl.2014.07.036

Watkins, J. M., Nielsen, L. C., Ryerson, F. J., & DePaolo, D. J. (2013). The influence of kinetics on the oxygen isotope composition of calcium carbonate. *Earth and Planetary Science Letters, 375*, 349-360. doi: http://dx.doi.org/10.1016/j.epsl.2013.05.054

Weber, J. N., & Raup, D. M. (1966). Fractionation of the stable isotopes of carbon and oxygen in marine calcareous organisms—the Echinoidea. Part I. Variation of C13 and O18 content within individuals. *Geochimica et Cosmochimica Acta, 30*(7), 681-703. doi: http://dx.doi.org/10.1016/0016-7037(66)90097-4

Weber, J. N., & Woodhead, P. M. J. (1970). Carbon and oxygen isotope fractionation in the skeletal carbonate of reef-building corals. *Chemical Geology, 6*, 93-117.

Zeebe, R. (1999a). An explanation of the effect of seawater carbonate concentration on foraminiferal oxygen isotopes. *Geochimica et Cosmochimica Acta, 63*, 2001-2007.

Zeebe, R. E. (2014). Kinetic fractionation of carbon and oxygen isotopes during hydration of carbon dioxide. *Geochimica et Cosmochimica Acta, 139*, 540-552. doi: http://dx.doi.org/10.1016/j.gca.2014.05.005

Zeebe, R. E., Bijma, J., & Wolf-Gladrow, D. A. (1999b). A diffusion-reaction model of carbon isotope fractionation in foraminifera. *Marine Chemistry, 64*(3), 199-227. doi: https://doi.org/10.1016/S0304-4203(98)00075-9

Zeebe, R. E., & Sanyal, A. (2002). Comparison of two potential strategies of planktonic foraminifera for house building: Mg^{2+} or H^{+} removal? *Geochimica et Cosmochimica Acta, 66*(7), 1159-1169. doi: https://doi.org/10.1016/S0016-7037(01)00852-3

Zeebe, R. E., & Wolf-Gladrow, D. (2001). *CO_2 in seawater: equilibrium, kinetics, isotopes* (Vol. 65). Amsterdam: Elsevier.

Zhang, J., Quay, P. D., & Wilbur, D. O. (1995). Carbon isotope fractionation during gas-water exchange and dissolution of CO_2. *Geochimica et Cosmochimica Acta, 59*, 107-114.

Zoccola, D., Tambutté, E., Kulhanek, E., Puverel, S., Scimeca, J.-C., Allemand, D., & Tambutté, S. (2004). Molecular cloning and localization of a PMCA P-type calcium ATPase from the coral Stylophora pistillata. *Biochimica et Biophysica Acta (BBA) - Biomembranes, 1663*(1), 117-126. doi: https://doi.org/10.1016/j.bbamem.2004.02.010